Powder Technology 299 (2016) 127–149

Contents lists available at ScienceDirect

Powder Technology

journal homepage: www.elsevier.com/locate/powtec

freepaper.me FREE paper

Heat transfer and entropy generation of natural convection on non-Newtonian nanofluids in a porous cavity

G.H.R. Kefayati *

School of Computer Science, Engineering and Mathematics, Flinders University, Adelaide, Australia

ARTICLE INFO

Article history:
Received 5 February 2016
Received in revised form 27 March 2016
Accepted 19 May 2016
Available online 25 May 2016

Keywords:
Natural convection
FDLBM
Non-Newtonian
Nanofluids
Porous cavity
Entropy generation

ABSTRACT

In this paper, heat transfer and entropy generation on laminar natural convection of non-Newtonian nanofluids in a porous square cavity have been analyzed by Finite Difference Lattice Boltzmann Method (FDLBM). The porous cavity is filled with water and nanoparticles of copper (Cu) while the mixture shows shear-thinning behavior. This study has been conducted for the certain pertinent parameters of Rayleigh number ($Ra = 10^4$–10^5), Darcy number ($Da = 0.001$, 0.01, and 0.1), and power-law index ($n = 0.6$–1), and the volume fraction has been studied from $\varphi = 0$ to 0.04. Results indicate that heat transfer and different irreversibilities enhance as Rayleigh number increases. The enhancement of the volume fraction augments heat transfer and the entropy generations due to heat transfer and fluid friction. The drop of the Darcy number causes the heat transfer and different entropy generations to decline considerably. Interestingly, the behavior of heat transfer and the studied entropy generations against the alteration of the power-law index is different in various Darcy numbers. In addition, the Bejan number demonstrates that the proportion of the irreversibilities due to heat transfer and fluid friction changes with the variation of the scrutinized parameters.

© 2016 Elsevier B.V. All rights reserved.

1. Introduction

1.1. Background

The fluids that are traditionally used for heat transfer applications such as water, mineral oils and ethylene glycol have a rather low thermal conductivity and they cannot play as an efficient heat transfer agent. Nanoparticles are known as an efficient way for improvement of thermal conductivity of base fluids. Fluids with nanoparticles suspended in them are called nanofluids. Nanofluids have anomalous high thermal conductivity at very low nanoparticles concentration and considerable enhancement of forced convective heat transfer. As a result, nanofluid has received high attention in heat transfer area. Flow in an enclosure driven by buoyancy force is a fundamental problem in fluid mechanics and heat transfer. This type of flow can be utilized as a validation in academic researches and various applications of engineering. Hence, several studies into natural convection of nanofluid have been conducted analytically, numerically and experimentally by different researchers [1–18]. On the other hand, the utilized cavity could be replaced simply with a porous cavity in some industries such as geothermal reservoirs, catalytic reactors, spreading of pollutants, solar collectors and interestingly, nanofluid is playing a crucial role in cooling and heating systems in the cited industries. As a result, several investigations have been conducted into the natural convection of nanofluid in porous enclosures recently. Sheremet and Pop [19] scrutinized steady-state natural convection heat transfer in a square porous enclosure having solid walls of finite thickness and conductivity filled by a nanofluid using the mathematical nanofluid model proposed by Buongiorno. Bourantas et al. [20] studied natural convection of a nanofluid in a square cavity filled with a porous matrix numerically using a meshless technique. The effect of the porous medium in the cooling efficiency of the nanofluidic system was discussed. Sheremet et al. [21] simulated transient natural convection in a porous wavy-walled cavity filled with a nanofluid. The main objective is to investigate the effects of the dimensionless time, thermal dispersion parameter and solid volume fraction parameters of nanoparticles on the fluid flow and heat transfer characteristics.

For the all of the mentioned numerical investigations, the base fluid was assumed to be Newtonian, but it is demonstrated that many nanofluids exhibit non-Newtonian, mainly shear-thinning behavior [22–29]. Therefore, it is necessary to be considered the effect of shear-thinning behavior of nanofluids. Moreover, the optimal design of heat transfer process in different industries is obtained with precision calculation of entropy generation since it clarifies energy losses in a system evidently. Hence, entropy generation is investigated into natural convection of pure fluids [30,31] and nanofluids in multifarious shapes extensively. Shahi et al. [32] studied the entropy generation induced by natural convection heat transfer in a square cavity containing Cu–

* GPO Box 2100, Adelaide, SA 5001, Australia.
E-mail addresses: gholamrezakefayati@gmail.com, gh.rkefayati@yahoo.com, gholamreza.kefayati@flinders.edu.au.

http://dx.doi.org/10.1016/j.powtec.2016.05.032
0032-5910/© 2016 Elsevier B.V. All rights reserved.

water nanofluid and a protruding heat source. It was found that the Nusselt number increased and the entropy generation reduced as the nanoparticle volume fraction was augmented. In addition, it was shown that the heat transfer performance could be maximized and the entropy generation minimized by positioning the heat source on the lower cavity wall. Esmaeilpour and Abdollahzadeh [33] examined the natural convection heat transfer behavior and entropy generation rate in a Cu–water nanofluid-filled cavity comprising two vertical wavy surfaces with different temperatures and two horizontal flat surfaces with thermal insulation. The results showed that the mean Nusselt number and entropy generation rate both decreased as the volume fractions of nanoparticles increased. It was also shown that the mean Nusselt number and rate of entropy generation increased with the rise of Grashof number, but decreased with the enhancement of the surface amplitude. Cho et al. [34] investigated the natural convection heat transfer performance and entropy generation rate in a water based nanofluid-filled cavity bounded by a left wavy-wall with a constant heat flux, a right wavy-wall with a constant low temperature, and flat upper and lower walls with adiabatic conditions. The results showed that the mean Nusselt number increased and the entropy generation rate decreased as the volume fraction of nanoparticles increased. Cho [35] performed a numerical simulation into heat transfer and entropy generation of natural convection in a partially-heated wavy-wall square cavity filled with Al_2O_3–water nanofluid. In the study, it was mentioned that the mean Nusselt number increases and the total entropy generation decreases as the volume fraction of Al_2O_3 nanoparticles increases. Sheikholeslami et al. [36] investigated nanofluid flow and heat transfer in a square enclosure containing a rectangular heated body computationally. The results indicated that both the Nusselt number and dimensionless entropy generation enhances when the Rayleigh number and nanoparticle volume fraction rise. Kefayati [37] analyzed heat transfer and entropy generation due to laminar natural convection in a square cavity filled with non-Newtonian nanofluid. It was found that entropy generation due to fluid friction and heat transfer rise as the Rayleigh number enhances. In addition, augmentation of volume fraction enhances entropy generations due to heat transfer and fluid friction in different power-law indexes.

Lattice Boltzmann method has been a powerful mesoscopic method in different subjects and shapes such as nanofluid, ferrofluid, MHD flow, porous medium, turbulent flow, melting and so on [38–50]. However, it does not have the considerable success in non-Newtonian fluid especially for non-isothermal problems. Hence, the simulation of the problem requires a special innovative numerical method which has the capacity to solve the problem accurately and efficiently while protects the merit of LBM. Therefore, Finite Difference Lattice Boltzmann Method (FDLBM) has been applied to solve the problem as it has the ability to derive the shear stresses equations in the form of the classical equations in contrast with Lattice Boltzmann Method (LBM). Independency of the method to the relaxation time in contrast with the common LBM causes the method to solve different non-Newtonian fluid energy equations successfully as the method protects the positive points of LBM simultaneously. In addition, the validation of the method and its mesh independency demonstrates that is more capable than conventional LBM. The method has been proposed by Fu et al. [51]. Moreover, Kefayati [52–70] developed and applied the FDLBM to simulate various complicated problems recently.

The main aim of this study is to simulate laminar natural convection of non-Newtonian nanofluid in a porous square cavity by FDLBM. It is endeavored to express the effect of different parameters on the flow and thermal fields. In addition, the energy management of the problem is analyzed by studying the entropy generations due to heat transfer and fluid friction as the proportions of the irreversibilities are investigated by the average Bejan number. The results of FDLBM are validated with previous numerical investigations and the effects of the main parameters (power-law index, volume fraction, Darcy number and Rayleigh number) on the flow and energy fields as well as the entropy generation are researched.

2. Problem statement

The geometry of the present problem is shown in Fig. 1. It consists of a two-dimensional cavity with the height of L. The temperature of the left wall has been considered to be maintained at high temperature of T_H as the right sidewall is kept at low temperature of T_C. The horizontal walls are adiabatic and impermeable. The porous cavity is filled with a non-Newtonian shear-thinning nanofluid of water/Cu where the pertinent thermophysical properties are given in Table 1. The general form of the momentum equation of incompressible fluid in saturated variable porosity can be derived by averaging the Navier–Stokes equations over the representative elementary volume (REV). The Brinkman-extended Darcy model without the inertia term is applied for the simulation of the porous media as it has been used in a large number of investigations for natural convection in rectangular porous enclosures [69–73]. Uniform porosity and permeability has been applied in this study. The ratios of the thermophysical properties of the porous medium and of the fluid, for the specific heat $\sigma = \frac{(\rho c_p)_m}{(\rho c_p)_f}$, for the thermal conductivity $R_k = \frac{k_m}{k_f}$, and for viscosity $\Lambda = \frac{\mu_m}{\mu_f}$ are equal to one. The flow is incompressible, steady, and laminar. It is assumed that nanoparticles are suspended in the nanofluid using either surfactant or surface charge technology. Further, it is assumed that the liquid and solid are in thermal equilibrium and they flow at the same velocity. The density variation is approximated by the standard Boussinesq model. In addition, the viscous dissipation in the energy equation has been neglected.

3. Theoretical formulation

3.1. Dimensional equations

Considering the above assumptions, the following governing equations are used to represent the flow phenomena [37,69].

$$\frac{\partial \overline{u}}{\partial \overline{x}} + \frac{\partial \overline{v}}{\partial \overline{y}} = 0 \tag{1}$$

$$\rho_{nf}\left(\frac{\partial \overline{u}}{\partial \overline{t}} + \overline{u}\frac{\partial \overline{u}}{\partial \overline{x}} + \overline{v}\frac{\partial \overline{u}}{\partial \overline{y}}\right) = -\frac{\partial \overline{P}}{\partial \overline{x}} + \left(\frac{\partial \overline{\tau}_{xx}}{\partial \overline{x}} + \frac{\partial \overline{\tau}_{xy}}{\partial \overline{y}}\right) - \frac{\overline{\mu}_{nf}}{K}\overline{u} \tag{2}$$

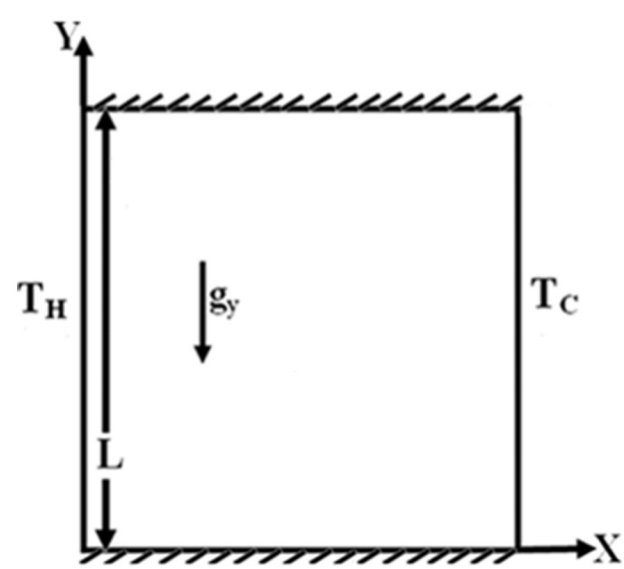

Fig. 1. Geometry of the present study.

freepaper.me FREE paper

Table 1
Thermophysical properties of water and copper.

Property	Fluid (water)	Solid (Cu)
c_p (j/kg k)	4179	383
ρ (kg/m^3)	997.1	8954
β (k^{-1})	2.1×10^{-4}	1.67×10^{-5}
k (w/m k)	0.613	400

$$\rho_{nf}\left(\frac{\partial \overline{v}}{\partial \overline{t}}+\overline{u}\frac{\partial \overline{v}}{\partial \overline{x}}+\overline{v}\frac{\partial \overline{v}}{\partial \overline{y}}\right)=-\frac{\partial \overline{P}}{\partial \overline{y}}+\left(\frac{\partial \overline{\tau}_{xy}}{\partial \overline{x}}+\frac{\partial \overline{\tau}_{yy}}{\partial \overline{y}}\right)+g(\rho\beta)_{nf}(T-T_C)-\frac{\overline{\mu}_{nf}}{K}\overline{v} \tag{3}$$

$$\frac{\partial \overline{T}}{\partial \overline{t}}+\overline{u}\frac{\partial \overline{T}}{\partial \overline{x}}+\overline{v}\frac{\partial \overline{T}}{\partial \overline{y}}=\alpha_{nf}\left(\frac{\partial^2 \overline{T}}{\partial \overline{x}^2}+\frac{\partial^2 \overline{T}}{\partial \overline{y}^2}\right) \tag{4}$$

α_{nf} is the thermal diffusivity of the nanofluid and it is given by [37].

$$\alpha_{nf}={}^{K_{nf}}/_{(\rho C_P)_{nf}} \tag{5}$$

The density, ρ_{nf}, the heat capacity, $(\rho c_p)_{nf}$, and the thermal expansion coefficient, $(\rho\beta)_{nf}$, of the nanofluid are obtained from the following respective equations [37]:

$$\rho_{nf}=(1-\varphi)\rho_f+\varphi\rho_s \tag{6}$$

$$(\rho c_p)_{nf}=(1-\varphi)(\rho c_p)_f+\varphi(\rho c_p)_s \tag{7}$$

$$(\rho\beta)_{nf}=(1-\varphi)(\rho\beta)_f+\varphi(\rho\beta)_s \tag{8}$$

With φ being the volume fraction of the solid particles and subscripts *f*, *nf* and *s* stand for base fluid, nanofluid and solid, respectively. The effective thermal conductivity of the spherical nanofluid can be approximated by the Maxwell–Garnetts (MG) model as [1–18]:

$$\frac{k_{nf}}{k_f}=\frac{k_s+2k_f-2\varphi(k_f-k_s)}{k_s+2k_f+\varphi(k_f-k_s)} \tag{9}$$

For a purely-viscous non-Newtonian nanofluid which follows the Ostwald–De Waele (i.e. power-law) model the shear stress tensor is

$$\overline{\tau}_{xx}=2\overline{\mu}_{nf}\frac{\partial \overline{u}}{\partial \overline{x}} \tag{10a}$$

$$\overline{\tau}_{yy}=2\overline{\mu}_{nf}\frac{\partial \overline{v}}{\partial \overline{y}} \tag{10b}$$

$$\overline{\tau}_{xy}=\overline{\tau}_{yx}=\overline{\mu}_{nf}\left(\frac{\partial \overline{u}}{\partial \overline{y}}+\frac{\partial \overline{v}}{\partial \overline{x}}\right) \tag{10c}$$

μ_{nf} is the effective dynamic viscosity of the nanofluid which is given as [1–18]:

$$\overline{\mu}_{nf}=\frac{\overline{\mu}_f}{(1-\varphi)^{2.5}} \tag{11}$$

where

$$\overline{\mu}_f=N\left\{2\left[\left(\frac{\partial \overline{u}}{\partial \overline{x}}\right)^2+\left(\frac{\partial \overline{v}}{\partial \overline{y}}\right)^2\right]+\left(\frac{\partial \overline{v}}{\partial \overline{x}}+\frac{\partial \overline{u}}{\partial \overline{y}}\right)^2\right\}^{\frac{(n-1)}{2}} \tag{12}$$

In the above equations $(\overline{u},\overline{v})$, $\overline{T}$ and $\overline{P}$ are the dimensional velocities, temperature and pressure respectively, ρ is density, N is the consistency coefficient and n is the power-law index. Therefore, the deviation of n from unity indicates the degree of deviation from Newtonian behavior. With $n \neq 1$, the constitute Eq. (12) represents pseudoplastic fluid ($n < 1$) and for ($n > 1$) it represents a dilatant fluid, respectively. Pseudoplastic fluids are characterized by an apparent viscosity which decreases with increasing shear rate, however in dilatant fluids the apparent viscosity increases with increasing shear rate.

The boundary conditions of the problem are as follows:

$$\text{Upper wall } \overline{y}=L,\ 0\le\overline{x}\le L,\ \overline{u}=\overline{v}=0,\frac{\partial \overline{T}}{\partial \overline{y}}=0 \tag{13a}$$

$$\text{Lower wall } \overline{y}=0,\ 0\le\overline{x}\le L,\ \overline{u}=\overline{v}=0,\frac{\partial \overline{T}}{\partial \overline{y}}=0 \tag{13b}$$

$$\text{Left wall } \overline{x}=0,\ 0\le\overline{y}\le L,\ \overline{u}=\overline{v}=0,\overline{T}=T_H \tag{13c}$$

$$\text{Right wall } \overline{x}=L,\ 0\le\overline{y}\le L,\ \overline{u}=\overline{v}=0,\overline{T}=T_C \tag{13d}$$

3.1.1. Entropy generation

In the studied problem, the irreversibility is generated through heat transfer and fluid flow. As a result, the total entropy is the sum of irreversibilities due to thermal gradients, viscous dissipation as follows [37]:

$$\overline{S}_S=\overline{S}_F+\overline{S}_T \tag{14}$$

where the entropy generations due to fluid flow ($\overline{S}_F$), and heat transfer ($\overline{S}_T$) are calculated as follows [37,69]:

$$\overline{S}_F=\frac{\overline{\mu}_{nf}}{T_0K}\left[\overline{u}^2+\overline{v}^2\right]+\frac{\overline{\mu}_{nf}}{T_0}\left[2\left(\frac{\partial \overline{u}}{\partial \overline{x}}\right)^2+2\left(\frac{\partial \overline{v}}{\partial \overline{y}}\right)^2+\left(\frac{\partial \overline{u}}{\partial \overline{y}}+\frac{\partial \overline{v}}{\partial \overline{x}}\right)^2\right] \tag{15}$$

$$\overline{S}_T=\frac{k_{nf}}{T_0^2}\left[\left(\frac{\partial \overline{T}}{\partial \overline{x}}\right)^2+\left(\frac{\partial \overline{T}}{\partial \overline{y}}\right)^2\right] \tag{16}$$

An important measure of the entropy field is Bejan number (Be) which is defined as the ratio between entropy generations due to heat transfer irreversibilities to the total entropy generation as follows [37, 69]:

$$\overline{Be}=\frac{\overline{S}_T}{\overline{S}_S} \tag{17}$$

3.2. Non-dimensional equations

In order to proceed to the numerical solution of systems (1)–(4) with the boundary conditions (13a), (13b), (13c) and (13d) the following non-dimensional variables are introduced.

$$x=\frac{\overline{x}}{L},\quad y=\frac{\overline{y}}{L},\quad u=\frac{\overline{u}}{\left(\frac{\alpha_f}{L}\right)Ra^{0.5}},\quad v=\frac{\overline{v}}{\left(\frac{\alpha_f}{L}\right)Ra^{0.5}},$$
$$P=\frac{\overline{P}}{\rho_{nf}\left(\frac{\alpha_f}{L}\right)^2Ra},\quad t=\frac{\overline{t}}{\left(\frac{L^2}{\alpha_f}\right)Ra^{-0.5}},\quad T=\frac{\overline{T}-T_C}{T_H-T_C}, \tag{18}$$

By substitution of Eq. (8) to Eqs. (1)–(4), the following system of equation is derived

$$\frac{\partial u}{\partial x}+\frac{\partial v}{\partial y}=0 \tag{19}$$

دانلود کننده مقالات علمی freepaper.me FREE paper

$$\left(\frac{\partial u}{\partial t}+u\frac{\partial u}{\partial x}+v\frac{\partial u}{\partial y}\right)=-\frac{\partial P}{\partial x}+\frac{\Pr}{\sqrt{Ra}}\frac{\rho_f}{\rho_{nf}}\frac{1}{(1-\varphi)^{2.5}}\left[2\frac{\partial}{\partial x}\left(\frac{\mu_f}{N}\frac{\partial u}{\partial x}\right)+\frac{\partial}{\partial y}\left(\frac{\mu_f}{N}\left(\frac{\partial u}{\partial y}+\frac{\partial v}{\partial x}\right)\right)\right]-\frac{\rho_f}{\rho_{nf}}\frac{1}{(1-\varphi)^{2.5}}\frac{\Pr}{Da\sqrt{Ra}}\frac{\mu_f}{N}u \tag{20}$$

$$\left(\frac{\partial v}{\partial t}+u\frac{\partial v}{\partial x}+v\frac{\partial v}{\partial y}\right)=-\frac{\partial P}{\partial y}+\frac{\Pr}{\sqrt{Ra}}\frac{\rho_f}{\rho_{nf}}\frac{1}{(1-\varphi)^{2.5}}\left[2\frac{\partial}{\partial y}\left(\frac{\mu_f}{N}\frac{\partial v}{\partial y}\right)+\frac{\partial}{\partial x}\left(\frac{\mu_f}{N}\left(\frac{\partial u}{\partial y}+\frac{\partial v}{\partial x}\right)\right)\right]+\Pr\frac{(\rho\beta)_{nf}}{\rho_{nf}\beta_f}T-\frac{\rho_f}{\rho_{nf}}\frac{1}{(1-\varphi)^{2.5}}\frac{\Pr}{Da\sqrt{Ra}}\frac{\mu_f}{N}v \tag{21}$$

$$\frac{\partial T}{\partial t}+u\frac{\partial T}{\partial x}+v\frac{\partial T}{\partial y}=\frac{1}{\sqrt{Ra}}\frac{\alpha_{nf}}{\alpha_f}\left(\frac{\partial^2 T}{\partial x^2}+\frac{\partial^2 T}{\partial y^2}\right) \tag{22}$$

$$\mu_f=N\left\{2\left[\left(\frac{\partial u}{\partial x}\right)^2+\left(\frac{\partial v}{\partial y}\right)^2\right]+\left(\frac{\partial v}{\partial x}+\frac{\partial u}{\partial y}\right)^2\right\}^{\frac{(n-1)}{2}} \tag{23}$$

The boundary conditions of the problem are

$$\text{Upper wall}\quad y=1,\quad 0\le x\le 1,\quad u=v=0,\frac{\partial T}{\partial y}=0 \tag{24a}$$

$$\text{Lower wall}\quad y=0,\quad 0\le x\le 1,\quad u=v=0,\frac{\partial T}{\partial y}=0 \tag{24b}$$

$$\text{Left wall}\quad x=0,\quad 0\le y\le 1,\quad u=v=0,T=1 \tag{24c}$$

$$\text{Right wall}\quad x=1,\quad 0\le y\le 1,\quad u=v=0,T=0 \tag{24d}$$

The non-dimensional parameters entering now into the problem under consideration are

$$Ra=\frac{\rho_f\beta_f g_y L^3(T_H-T_C)}{\mu_f\ \alpha_f}\text{(Rayleigh number)} \tag{25}$$

$$\Pr=\frac{\mu_f}{\rho_f\ \alpha_f}\text{(Prandtl number)} \tag{26}$$

$$Da=\frac{K}{L^2}\text{(Darcy number)} \tag{27}$$

3.2.1. Entropy generation

The dimensionless entropy generation with consideration to non-dimensional variables can be acquired as follows [37]:

$$S_S=S_F+S_T \tag{28}$$

$$S_S=\overline{S}_S\times\frac{T_0{}^2L^2}{k_{nf}\Delta T^2} \tag{29}$$

$$S_F=\Phi_I\left[u^2+v^2+Da\left[2\left(\frac{\partial u}{\partial x}\right)^2+2\left(\frac{\partial v}{\partial y}\right)^2+\left(\frac{\partial u}{\partial y}+\frac{\partial v}{\partial x}\right)^2\right]\right] \tag{30}$$

$$S_T=\frac{k_{nf}}{k_f}\left[\left(\frac{\partial T}{\partial x}\right)^2+\left(\frac{\partial T}{\partial y}\right)^2\right] \tag{31}$$

$$\Phi_I=\frac{\mu_{nf}T_0}{k_f}\left(\frac{\alpha_f}{L\Delta T}\right)^2Ra=\frac{\left\{2\left[\left(\frac{\partial u}{\partial x}\right)^2+\left(\frac{\partial v}{\partial y}\right)^2\right]+\left(\frac{\partial v}{\partial x}+\frac{\partial u}{\partial y}\right)^2\right\}^{\frac{(n-1)}{2}}T_0}{(1-\varphi)^{2.5}\times k_f}\left(\frac{\alpha_f}{L\Delta T}\right)^2Ra \tag{32a}$$

$$\Phi_I=\frac{Ra\left\{2\left[\left(\frac{\partial u}{\partial x}\right)^2+\left(\frac{\partial v}{\partial y}\right)^2\right]+\left(\frac{\partial v}{\partial x}+\frac{\partial u}{\partial y}\right)^2\right\}^{\frac{(n-1)}{2}}}{(1-\varphi)^{2.5}}\lambda \tag{32b}$$

$$\lambda=\frac{T_0}{k_f}\left(\frac{\alpha_f}{L\Delta T}\right)^2 \tag{33}$$

The non-dimensional Bejan number is calculated as follows:

$$Be=\frac{S_T}{S_S} \tag{34}$$

It should be mentioned that the variable of λ is taken constant and it is 0.01.

The total dimensionless entropy generations and average Bejan number are obtained by numerical integration of the local dimensionless entropy generation over the entire cavity volume. It is given by:

$$SF=\int_0^1\int_0^1 S_F dxdy\ ,\ ST=\int_0^1\int_0^1 S_T dxdy,\ SS=\int_0^1\int_0^1 S_S dxdy \tag{35a}$$

$$Be_{avg}=\int_0^1\int_0^1 Be\ dxdy \tag{35b}$$

4. Finite Difference Lattice Boltzmann Method (FDLBM)

The normalized discrete Boltzmann equation can be written as follows:

$$\frac{\partial f_\alpha}{\partial t}+\xi_\alpha.\nabla f_\alpha=-\frac{1}{\varepsilon\phi}\left(f_\alpha-f_\alpha^{eq}\right) \tag{36}$$

where ϕ, ξ_α, f_α and f_α^{eq} are the relaxation time, the discrete particle velocity, the discrete particle distribution function, and the discrete particle equilibrium distribution function, respectively. Moreover, ε is a small parameter, which is taken as a time step $\varepsilon=\Delta t$. The idea of changing the equilibrium distribution function (f_α^{eq}) instead of changing the relaxation time (ϕ) has been employed in this method. In fact, since the relaxation time (ϕ) is arbitrary in the present method and it always appears together with ε, using an appropriate normalization ϕ can always be treated as unity.

If a splitting method has been applied on the Eq. (36) and setting the relaxation time equals one ($\phi=1$), the streaming stage can be mentioned as

$$\frac{\partial f_\alpha}{\partial t}+\xi_\alpha.\nabla_x f_\alpha=0 \tag{37}$$

Eq. (37) has been solved by a Lax–Wendroff (LW) scheme [74]. The collision step that has been created by the splitting method is as

$$\frac{\partial f_\alpha}{\partial t}=-\frac{1}{\varepsilon\phi}\left(f_\alpha(x,t)-f_\alpha^{eq}(x,t)\right) \tag{38}$$

The solution of the streaming step will serve as initial conditions for the solution of the collision step. Eq. (38) can be simplified by using the Euler method and the choice of $\varepsilon=\Delta t$ and $\phi=1$,

$$\frac{f_\alpha(x,t+\Delta t)-f_\alpha(x,t)}{\Delta t}=-\frac{1}{\varepsilon\phi}\left(f_\alpha(x,t)-f_\alpha^{eq}(x,t)\right) \tag{39}$$

then,

$$f_\alpha(x,t+\Delta t)=f_\alpha^{eq}(x,t) \tag{40}$$

The equilibrium distribution function (f_α^{eq}) is different from conventional ones adopted by previous researchers, who normally expand the

FREE paper freepaper.me دانلود کننده مقالات علمی

Maxwellian distribution function up to the second or third order in terms of the products of u and ξ_α.The present approach proposes a polynomial in terms of ξ_α as follows [51]:

$$f_\alpha^{eq} = A_\alpha + (\xi_\alpha)_x Ax_\alpha + (\xi_\alpha)_y Ay_\alpha + (\xi_\alpha)_x^2 Bxx_\alpha + (\xi_\alpha)_y^2 Byy_\alpha + (\xi_\alpha)_x(\xi_\alpha)_y Bxy_\alpha. \tag{41}$$

where ξ_α for a D2Q9 can be stated as (Fig. 2)

$$\xi_a = \begin{cases} 0 & \alpha = 0 \\ c(\cos[(i-1)^\pi/_2], \sin[(i-1)^\pi/_2]) & \alpha = 1,3,5,7 \\ c\sqrt{2}(\cos[(i-5)^\pi/_2 + {}^\pi/_4], \sin[(i-5)^\pi/_2 + {}^\pi/_4]) & \alpha = 2,4,6,8 \end{cases} \tag{42}$$

c is a special parameter which should be specified with consideration to other parameters. Since the value of c affects numerical stability, it is modified in each step. The modified equation is as follows [51]:

$$c = \sqrt{\left|u^2 + v^2 - \frac{2p}{\rho}\right|} \tag{43}$$

Other parameters in the equilibrium distribution function (f_α^{eq}) with consideration are defined as

$$A_0 = \rho - \frac{2p}{c^2} - \frac{\rho|u|^2}{c^2} + \frac{\tau_{xx} + \tau_{yy}}{c^2}, A_1 = A_2 = 0 \tag{44a}$$

$$Ax_1 = \frac{\rho u}{2c^2}, \quad Ax_2 = 0 \tag{44b}$$

$$Ay_1 = \frac{\rho v}{2c^2}, \quad Ay_2 = 0 \tag{44c}$$

$$Bxx_1 = \frac{1}{2c^4}(p + \rho u^2 - \tau_{xx}), \quad Bxx_2 = 0 \tag{44d}$$

$$Byy_1 = \frac{1}{2c^4}(p + \rho v^2 - \tau_{yy}), \quad Byy_2 = 0 \tag{44e}$$

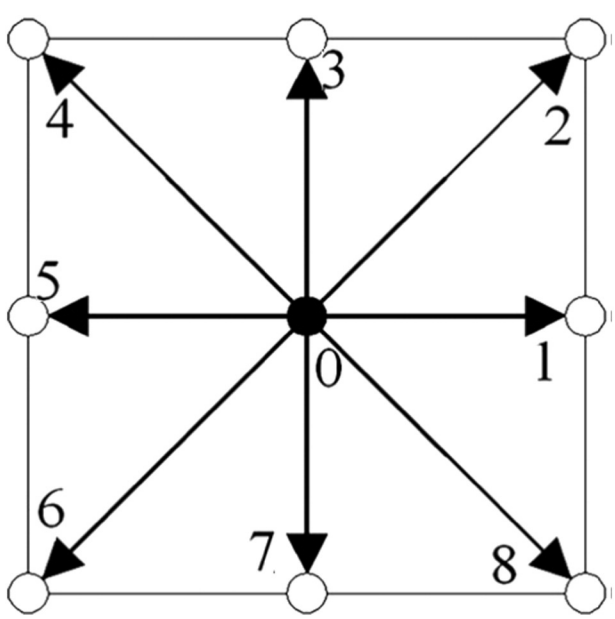

Fig. 2. Discrete velocity distribution in D2Q9.

$$Bxy_2 = \frac{1}{4c^4}(\rho vu - \tau_{xy}), \quad Bxy_1 = 0, \quad i,j = x,y \tag{44f}$$

Assuming parameters with the same magnitude of ξ_α to be equal, the coefficients in Eq. (41), A_α, Ax_α, Ay_α, etc., can be simplified to give the following:

$$\begin{aligned} &A_1 = A_3 = A_5 = A_7; && A_2 = A_4 = A_6 = A_8 \\ &Ax_1 = Ax_3 = Ax_5 = Ax_7, && Ax_2 = Ax_4 = Ax_6 = Ax_8 \\ &Ay_1 = Ay_3 = Ay_5 = Ay_7, && Ay_2 = Ay_4 = Ay_6 = Ay_8 \\ &Bxx_1 = Bxx_3 = Bxx_5 = Bxx_7, && Bxx_2 = Bxx_4 = Bxx_6 = Bxx_8 \\ &Byy_1 = Byy_3 = Byy_5 = Byy_7, && Byy_2 = Byy_4 = Byy_6 = Byy_8 \\ &Bxy_1 = Bxy_3 = Bxy_5 = Bxy_7, && Bxy_2 = Bxy_4 = Bxy_6 = Bxy_8 \end{aligned} \tag{45}$$

$$\tau_{xx} = \frac{2\,\mathrm{Pr}}{N\sqrt{\mathrm{Ra}}}\frac{1}{\rho_{nf}}\frac{\mu_f}{(1-\varphi)^{2.5}}\left(\frac{\partial u}{\partial x}\right) \tag{46a}$$

$$\tau_{yy} = \frac{2\,\mathrm{Pr}}{N\sqrt{\mathrm{Ra}}}\frac{1}{\rho_{nf}}\frac{\mu_f}{(1-\varphi)^{2.5}}\left(\frac{\partial v}{\partial y}\right) \tag{46b}$$

$$\tau_{yx} = \tau_{xy} = \frac{\mathrm{Pr}}{N\sqrt{\mathrm{Ra}}}\frac{1}{\rho_{nf}}\frac{\mu_f}{(1-\varphi)^{2.5}}\left(\frac{\partial u}{\partial y} + \frac{\partial v}{\partial x}\right) \tag{46c}$$

For the force terms in the momentum equation, the followed Eqs. (47)–(48) should be added to the streaming stage.

$$F_\alpha = A_\alpha + (\xi_\alpha)_x Ax_\alpha + (\xi_\alpha)_y Ay_\alpha \tag{47}$$

$$\begin{aligned} &A_0 = A_1 = A_2 = 0 \\ &Ax_1 = \frac{-\frac{\rho_f}{\rho_{nf}}\frac{1}{(1-\varphi)^{2.5}}\frac{\mathrm{Pr}}{Da\sqrt{\mathrm{Ra}}}\frac{\mu_f}{N}u}{2c^2}, Ax_2 = 0 \\ &Ay_1 = \frac{\mathrm{Pr}\frac{(\rho\beta)_{nf}}{\rho_{nf}\beta_f}T - \frac{\rho_f}{\rho_{nf}}\frac{1}{(1-\varphi)^{2.5}}\frac{\mathrm{Pr}}{Da\sqrt{\mathrm{Ra}}}\frac{\mu_f}{N}v}{2c^2}, Ay_2 = 0 \end{aligned} \tag{48}$$

The distribution function for energy (g_α^{eq}) can be obtained like the flow field and just the corresponding polynomials of the equilibrium distribution functions are different and they can be proposed as follows:

Energy:

$$g_\alpha^{eq} = A_\alpha + (\xi_\alpha)_x Ax_\alpha + (\xi_\alpha)_y Ay_\alpha \tag{49}$$

$$\begin{aligned} &A_0 = T \quad A_1 = A_2 = 0 \\ &Ax_1 = \frac{\left(uT - \frac{\alpha_{nf}}{\alpha_f}\frac{1}{\sqrt{\mathrm{Ra}}}\frac{\partial T}{\partial x}\right)}{2c^2}, \quad Ax_2 = 0 \\ &Ay_1 = \frac{\left(vT - \frac{\alpha_{nf}}{\alpha_f}\frac{1}{\sqrt{\mathrm{Ra}}}\frac{\partial T}{\partial y}\right)}{2c^2}, \quad Ay_2 = 0 \end{aligned} \tag{50}$$

The local and the average Nusselt numbers at the hot wall with the utilization of the dimensionless parameters are calculated as

$$NU_h = \left(-\frac{\partial T}{\partial x}\right)_{x=0} \tag{51}$$

$$NU_{avg} = \int_0^1 NU_h dy \tag{52}$$

Because of considering nanoparticles effects on different parameters exactly, normalized average Nusselt number on the hot wall is defined.

FREE paper freepaper.me دانلود کننده مقالات علمی

Table 2
Grid independence study at $Ra = 10^5$, $\varphi = 0$, $Da = 0.001$ and $n = 0.6$.

Mesh size	NU_{avg}
100 × 100	2.257
110 × 110	2.126
120 × 120	2.054
130 × 130	1.983
140 × 140	1.941
150 × 150	1.934
160 × 160	1.934

The normalized average Nusselt number express Nusselt number at any volume fractions to the pure fluid which is written as follows:

$$NU^*_{avg}(n) = \frac{NU_{avg}(\varphi)}{NU_{avg}(\varphi = 0)} \tag{53}$$

5. Code validation and grid independence

Finite Difference Lattice Boltzmann Method (FDLBM) scheme is utilized to obtain the numerical simulations of laminar natural convection in a porous cavity that is filled with non-Newtonian nanofluid while

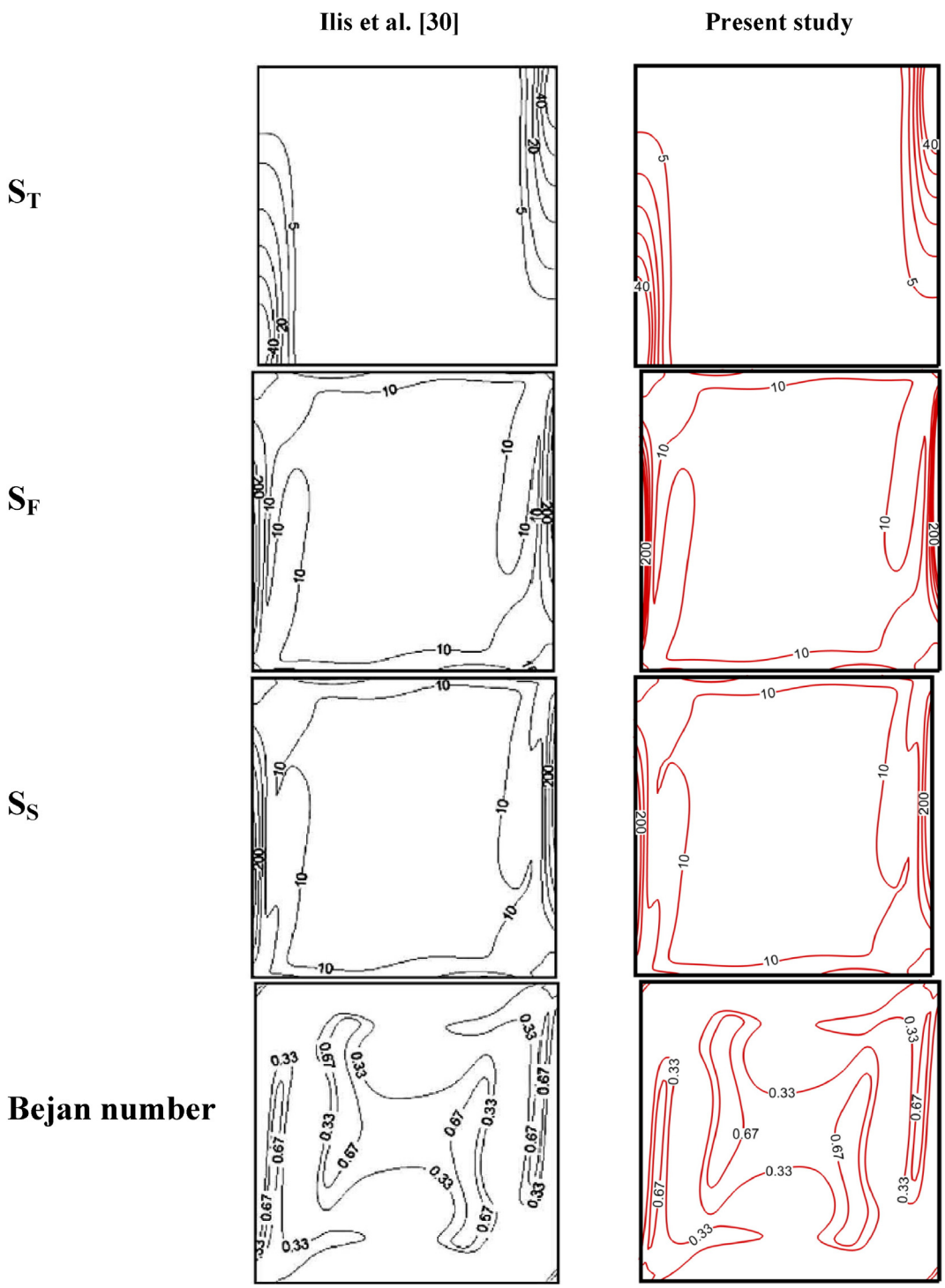

Fig. 3. Comparison between present study and Ilis et al. [30].

دانلود کننده مقالات علمی freepaper.me FREE paper

entropy generation has been studied in details as well. This problem was investigated at different Rayleigh numbers of (Ra = 10^4, and 10^5), Darcy numbers of Da = 0.001, 0.01, and 0.1, power-law index between 0.6 and 1, and volume fraction between $\varphi = 0$ to 0.04. An extensive mesh testing procedure was conducted to guarantee a grid independent solution. Seven different mesh combinations were explored for the case of Ra = 10^5, n = 1, Da = 0.001 and $\varphi = 0$. The present code was tested for grid independency by calculating the u and v velocities in the middle of the cavity as the average Nusselt on the hot wall has been studied. It was confirmed that the grid size (150_150) ensures a grid independent solution as portrayed by Table 2. Moreover, the FDLBM is applied for non- Newtonian natural and mixed convection of pure fluid and nanofluid in the presence and absence of mass transfer by the author recently [55–70] which demonstrates the accuracy of the utilized code properly. To check the precision of the present consequences for calculation of entropy, the obtained results were validated with the study of Ilis et al. [30] in Fig. 3.

6. Results and discussion

6.1. Effects of power-law index, Darcy number, and volume fraction on heat transfer and fluid flow

Fig. 4 provides comparisons of the isotherms between the base fluid ($\varphi = 0$) and the nanofluid ($\varphi = 0.04$) for different power-law indexes, and Darcy numbers at Ra = 10^5.

At Da = 10^{-3}, it is observed that the rise of power-law index causes the density of the base fluid isotherms on the hot wall to augment. In fact, it exhibits that the growth of power-law index enhances the convection process generally. The effect is more considerable at the isotherm of close to the bottom left side of the cavity where the increase in the power-law index provokes the movement of the isotherm between the cold and hot walls to augment. The comparison between the base fluid and nanofluid in the isotherms clarify that the nanofluid isotherms incline to the hot wall more than the base fluid and therefore

FREE paper freepaper.me دانلود کننده مقالات علمی

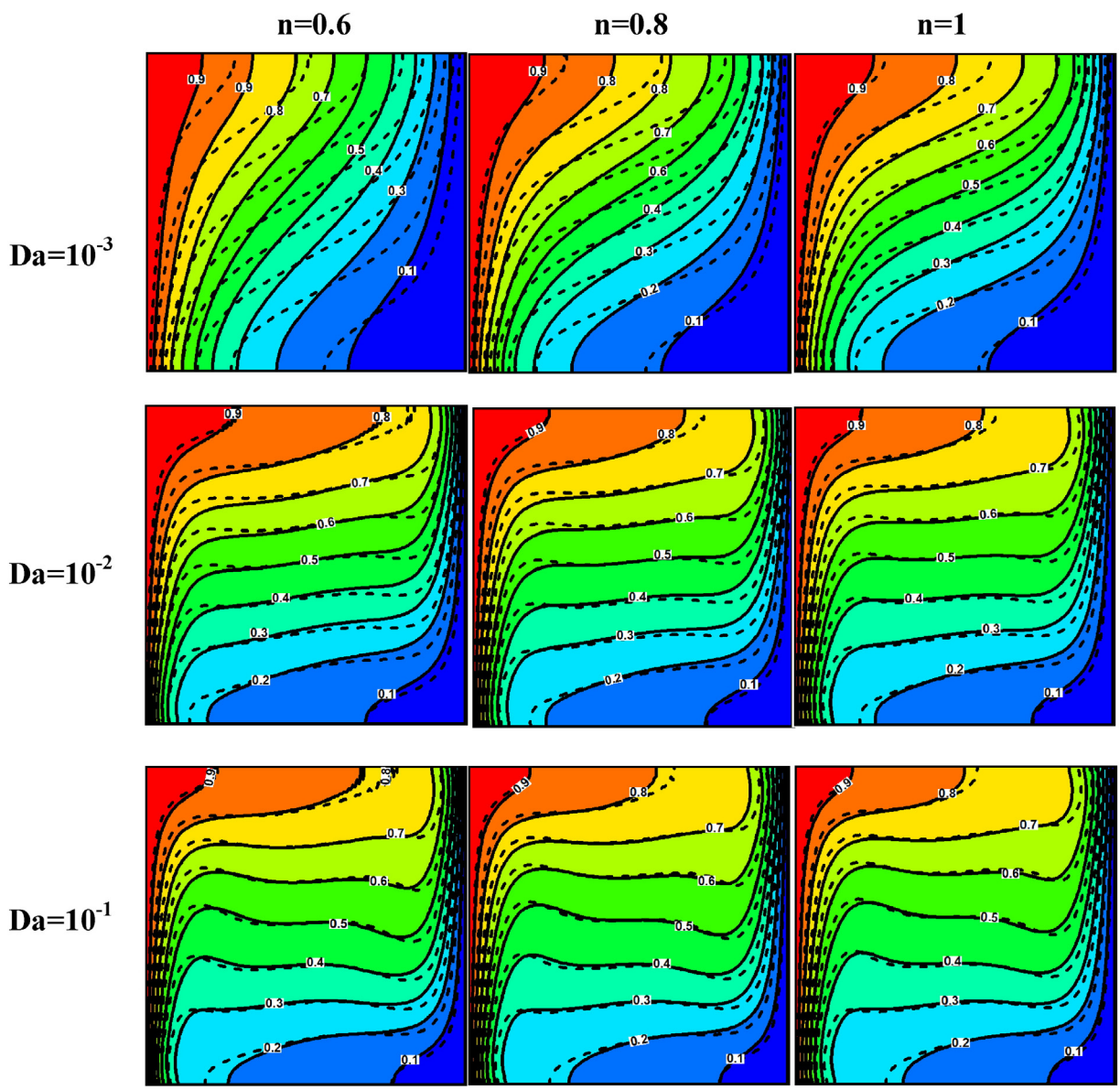

Fig. 4. Comparison of the isotherms between the base fluid (—) ($\varphi = 0$) and nanofluids (- - -) ($\varphi = 0.04$) for various power-law indexes and Darcy numbers at Ra = 10^5.

it proves that heat transfer increases in the presence of the nanoparticles.

At Da = 10^{-2}, the increase in the Darcy number causes the convection process to ameliorate significantly as the gradient of the isotherms on the hot wall and the movement of the isotherms between the cold and hot walls enhances. The effects of nanoparticles on the isotherms are similar to the Darcy number of Da = 0.001 as the isotherms of nanofluids become closer to the hot wall and enhance the convection process. In addition, the effects of nanopaticles on isotherms change as a reslut of the augmentation of Darcy number clearly. It is evident that the influences of nanoparticles drop as the Darcy number increases from Da = 0.001 to 0.01, although the drop is marginal. In contrast with the Darcy number of Da = 0.001, the increase in the power-law index declines the gradient temperature on the hot wall and therefore heat transfer.

At Da = 10^{-1}, the rise of the Darcy number from Da = 0.01 to 0.1 enhances the convection process as the gradient of the isotherms on the hot wall keeps increasing and the flow of the isotherms between the cold and hot walls grows. The trend of the nanoparticle influence on the isotherms is similar to the smaller Darcy numbers where the isotherms of nanofluids augment the convection process. Further, the effects of nanopaticles on isotherms alter due to the augmentation of Darcy number clearly since it indicates that the influences of nanoparticles drop as the Darcy number rises from Da = 0.01 to 0.1, but the decrease is minimal. It also demonstrates that the increase in the power-law index declines the gradient temperature on the hot wall and therefore heat transfer at Da = 0.01 more than Da = 0.1.

Fig. 5 draws comparisons of the streamlines between the base fluid ($\varphi = 0$) and the nanofluid ($\varphi = 0.04$) for different power-law indexes, and Darcy numbers at Ra = 10^5. Generally, the streamlines display the

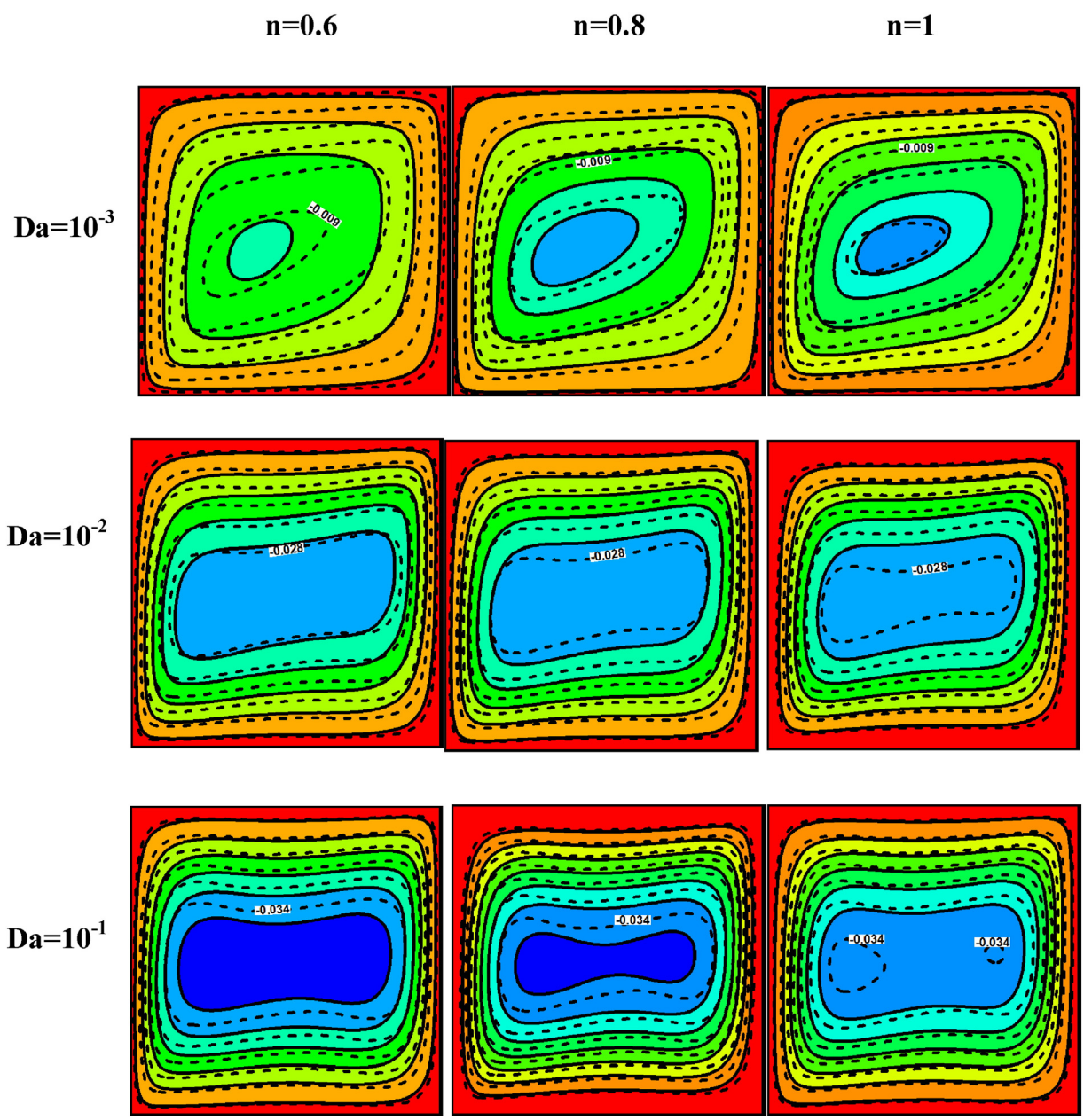

Fig. 5. Comparison of the streamlines between the base fluid (—) ($\varphi = 0$) and nanofluids (- - -) ($\varphi = 0.04$) for various power-law indexes and Darcy numbers at Ra = 10^5.

FREE paper freepaper.me دانلود کننده مقالات علمی

effects of nanofluid evidently as they become bigger compared to the streamlines of the base fluid. In other words, the augmentation of convection process because of the addition of nanoparticles provokes the streamlines to move in a bigger elliptic way in the cavity for multifarious studied power-law indexes and Darcy numbers. Moreover, the increase in the Darcy number improves the convection process as the streamlines move a bigger circle and pathway in the cavity evidently. In addition, the effect of the power-law index is evident in different Darcy numbers with a certain streamline in the core of the cavity. At Da = 0.001, the enhancement of power-law index causes the certain streamline of $\psi = -0.009$ to become bigger and demonstrates the improvement of the convection process as a result of the increase in the power-law index. On the other hand, a different pattern is observed against the rise of the power-law index on the streamlines at Da = 0.01 where the specific streamline of $\psi = -0.028$ diminishes with the augmentation of the power-law index. The trend is also apparent at Da = 0.1 where the streamline of $\psi = -0.034$ becomes smaller with the enhancement of power-law index. The pattern demonstrates that the convection process is weakened by the enhancement of the power-law index at Da = 0.01 and 0.1.

Fig. 6 displays the distribution of local Nusselt number on the hot wall and the local temperature in the middle of the cavity at y = 0.5

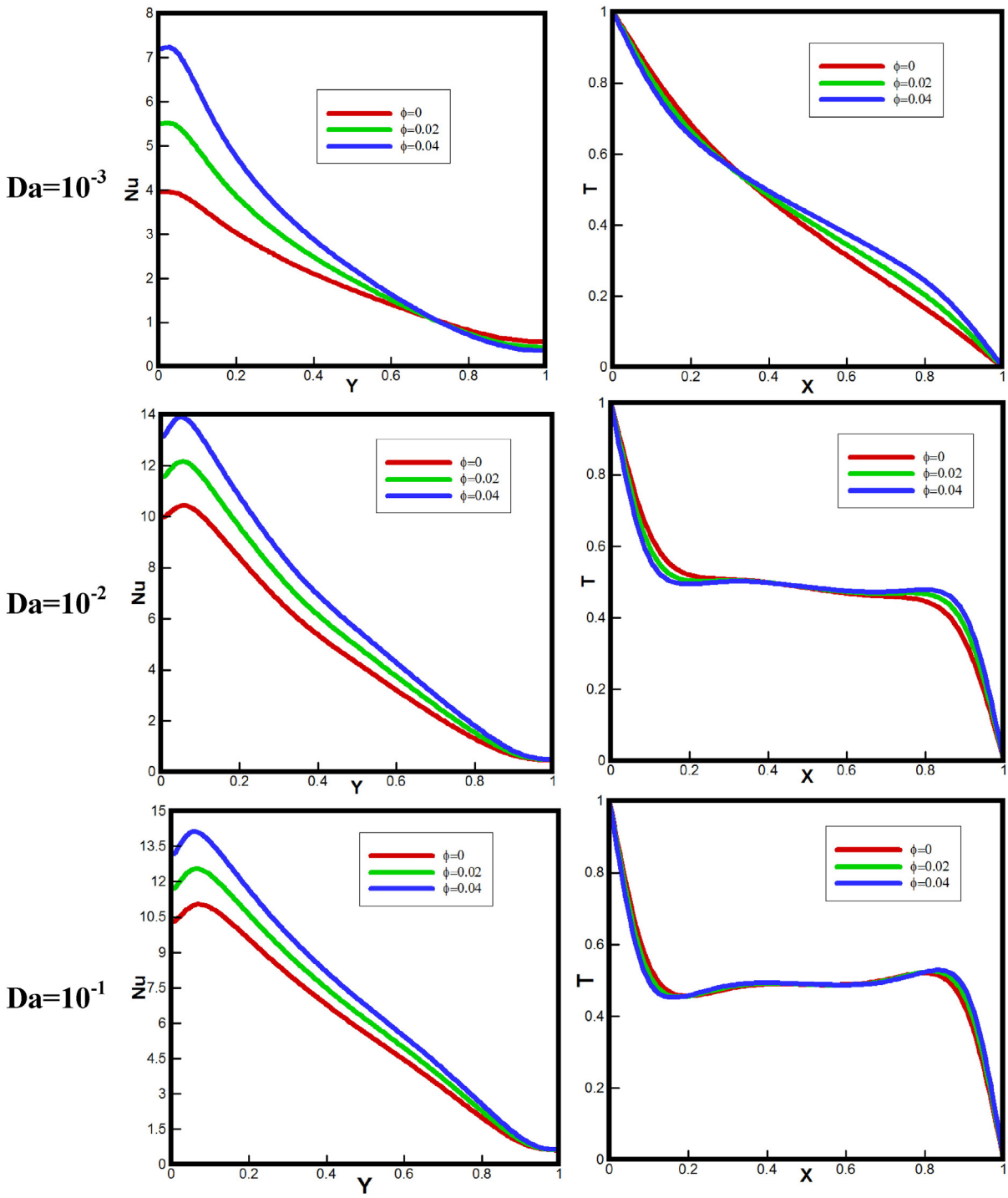

Fig. 6. Comparisons of local Nusselt number on the hot wall, and the temperature in the middle of the cavity at Y = 0.5 for different volume fractions and Darcy numbers at Ra = 10^5 and n = 0.6.

FREE paper freepaper.me دانلود کننده مقالات علمی

for different volume fractions and Darcy numbers at Ra = 10^5 and n = 0.6. It is clear that the local Nusselt number increases gradually as volume fraction augments. In addition, it shows that the local temperature in the middle of the cavity rises with the increase in volume fraction. The phenomenon demonstrates the convection process becomes stronger with the addition of the nanoparticles. Further, the local Nusselt number decreases as Darcy number drops gradually. Moreover, it illustrates that the rise of Darcy number causes the difference between the local Nusselt numbers of various volume fractions on the first part of the hot wall to drop. Also, the smooth line in the middle of the cavity at Da = 0.1 changes to a linear pattern steadily at Da = 0.001 with the decrease in Darcy number.

Fig. 7 shows the distribution of local Nusselt number on the hot wall and the temperature in the middle of the cavity at y = 0.5 for different power-law indexes and Darcy numbers at Ra = $10^5$and $\varphi = 0$. Generally, the values of the local Nusselt number without consideration to the values of the power-law index and the volume fraction decreases as the Darcy number falls. The phenomenon is confirmed by the trend of the temperature in the middle of the cavity where the curved and smooth line at Da = 0.1 alters to a linear one at Da = 0.001 and

FREE paper freepaper.me دانلود کننده مقالات علمی

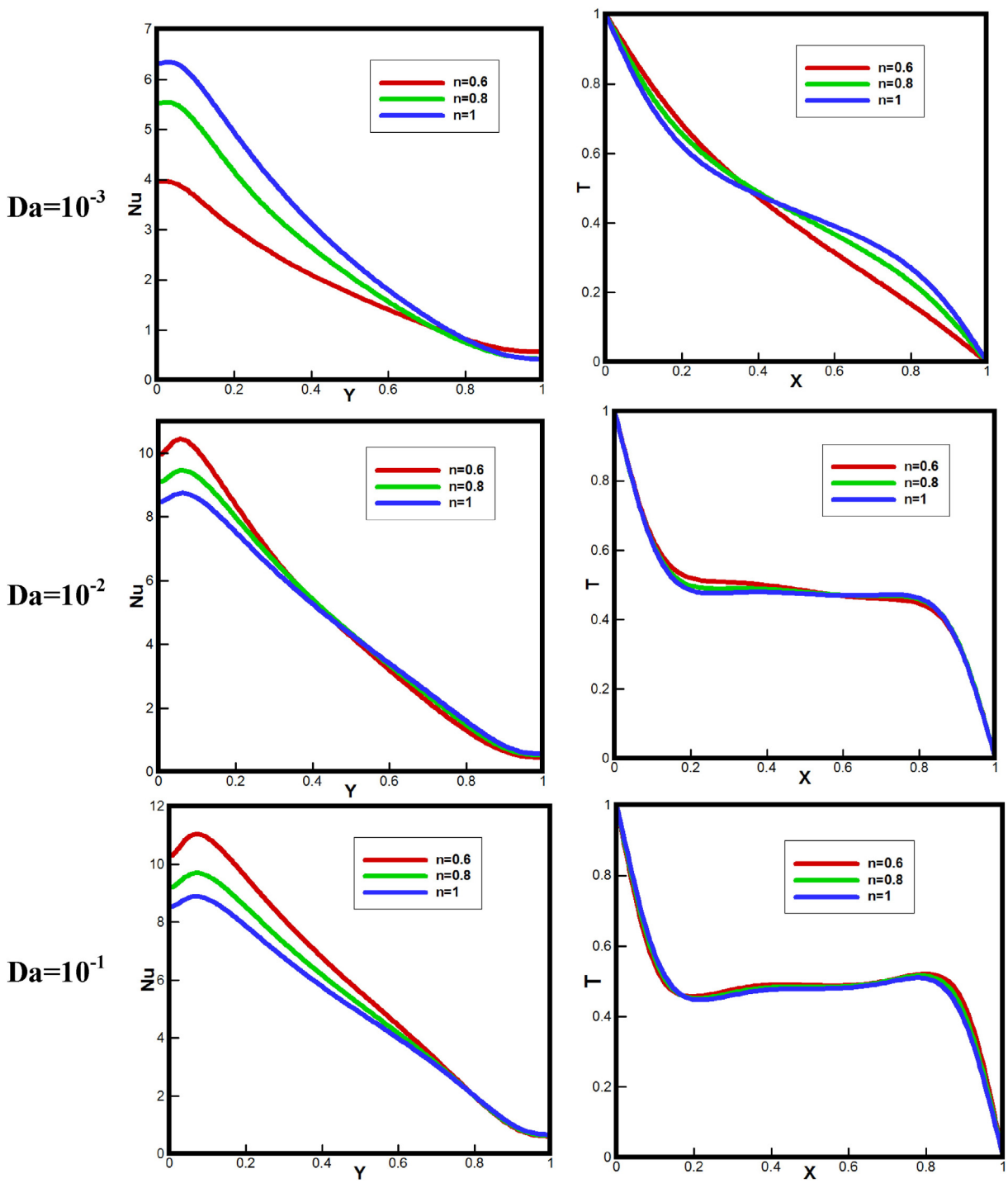

Fig. 7. Comparisons of local Nusselt number on the hot wall, and temperature in the middle of the cavity at Y = 0.5 for different power-law indexes and Darcy numbers at Ra = $10^5$and $\varphi = 0$.

demonstrates the weakness of convection and heat transfer. At Da = 0.001, it exhibits that the augmentation of power-law index causes the local Nusselt number to rise at Y < 0.8 while it drops slightly at Y > 0.8. However, it illustrates that the augmentation is not uniform where the greatest rise is observed from n = 0.6 to 0.8 and then the enhancement becomes smaller as the power-law index increases from n = 0.8 to 1. On the other hand, the local Nusselt number drops as the power-law index enhances in the first half of the hot wall at Da = 0.01 and 0.1. Moreover, it should be noted that the drop is more considerable at Da = 0.1. It is noticeable that the effect of the power-law index on the local Nusselt number is insignificant at Y > 0.6 for Da = 0.01 and 0.1. The temperature in the middle of the cavity at Da = 0.001 changes from a curved shape at n = 1 to a linear one at n = 0.6. It clearly indicates that the convection process weakens as the power-law index decreases at Da = 0.001. But, it is observable that the temperature in the middle of the cavity increases marginally with the decrease in the power-law index.

Fig. 8 indicates the average Nusselt number and the dimensionless average Nusselt number for different Rayleigh numbers, Darcy numbers, power-law indexes, and volume fractions. It is evident that the average Nusselt number enhances as the Rayleigh number rises for different power-law indexes and volume fractions. In addition, the enhancement of volume fraction in various power-law indexes and Rayleigh numbers provokes the average Nusselt number to augment. However, the effect of power-law index in multifarious Darcy numbers is different. Moreover, the effect of the nanoparticle on the increase in heat transfer is different for various power-law indexes, Darcy and Rayleigh numbers. The dimensionless average Nusselt number can clarify the influence of the nanoparticle at different studied parameters evidently. As a result, the parameters have been studied for each Darcy number. At Da = 0.001, the increase in the power-law index enhances the average Nusselt numbers in different Rayleigh numbers and volume fractions. The enhancement is more significant at Ra = 10^5 compared to Ra = 10^4. In addition, the non-dimensional average Nusselt number discloses that the effect of the nanoparticle enhances with the rise of the power-law index at Ra = 10^4, but, by contrast, the influence drops as the power-law index increases at Ra = 10^5 obviously. At Da = 0.01, the rise of the power-law index enhances the average Nusselt numbers in different volume fractions at Ra = 10^4; conversely, the increase in the power-law index causes the average Nusselt number to drop at Ra = 10^5. However, the non-dimensional average Nusselt number exhibits that the effect of the nanoparticle enhances with the drop of the power-law index in various Rayleigh numbers. At Da = 0.1, the decline of the power-law index augments the average Nusselt numbers in different Rayleigh numbers and volume fractions. The augmentation is more noteworthy at Ra = 10^5 compared to 10^4. Furthermore, the non-dimensional average Nusselt number

FREE paper freepaper.me دانلود کننده مقالات علمی

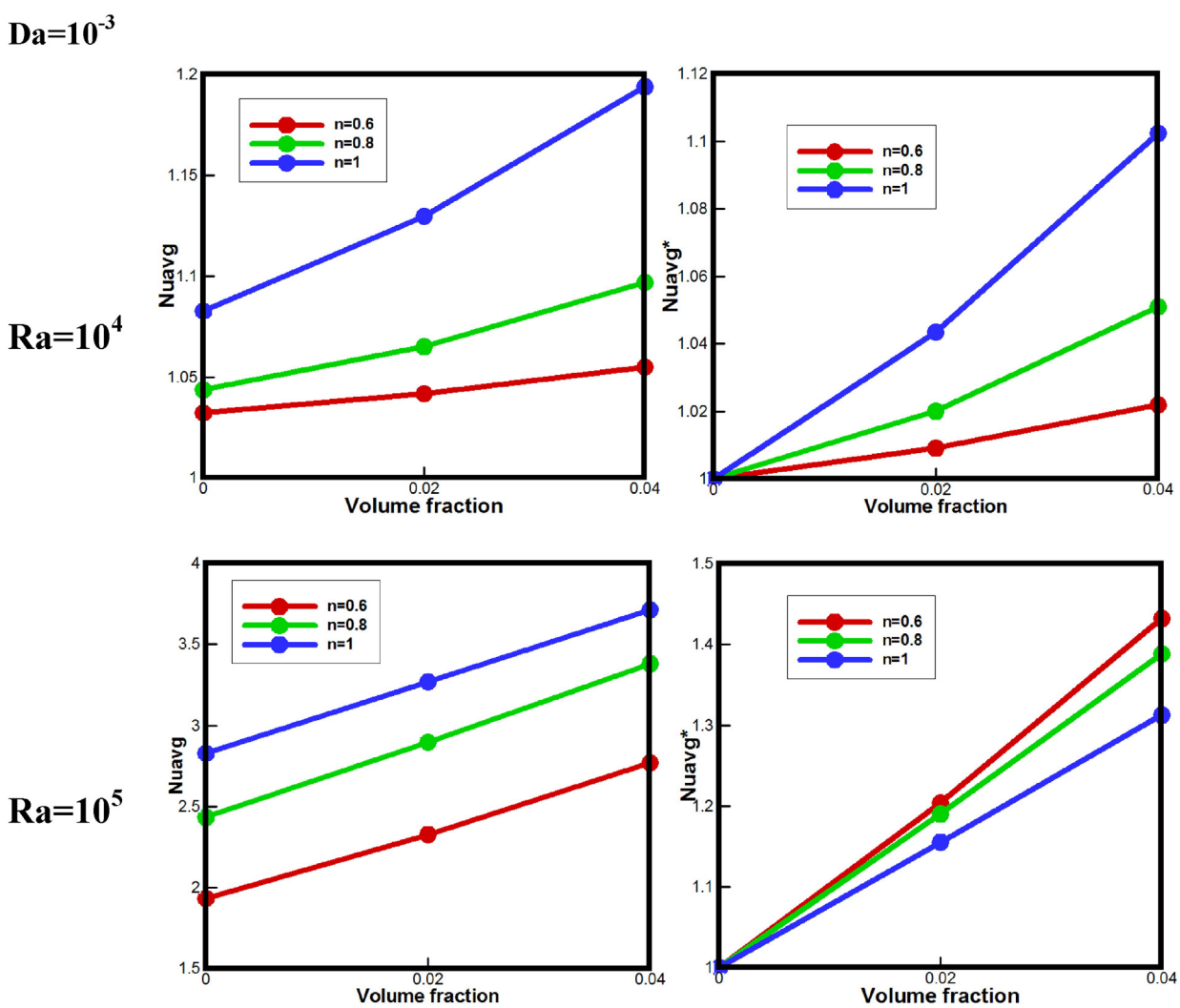

Fig. 8. Comparison between the average Nusselt and dimensionless average Nusselt numbers for various Rayleigh numbers, Darcy numbers, power-law indexes, and volume fractions.

reveals that the effect of nanoparticle declines with the rise of the power-law index for both studied Rayleigh numbers

6.2. Effects of power-law index, Darcy number, Rayleigh number and volume fraction on entropy generation due to heat transfer

Fig. 9 illustrates the local entropy generation due to heat transfer for pure fluid ($\varphi = 0$) and nanofluid ($\varphi = 0.04$) in different power-law indexes and Darcy numbers at Ra $= 10^5$ as maximum values of the local entropy generation is mentioned to provide a clear comparison between them. It illustrates that the enhancement of Darcy number augments the entropy generation generally in multifarious power-law indexes, Rayleigh numbers and volume fractions. It is evident that the maximum value of the irreversibility due to heat transfer occurs close to the sidewalls where the gradient of temperature is higher in these sections. It shows that the enhancement of power-law index results in the increase in the entropy generation. The maximum value of the local entropy generation and the contour of the local entropy generation demonstrate that the addition of nanoparticles enhances entropy generation due to heat transfer for various power-law indexes and Darcy numbers. Nevertheless, the contours and the maximum values indicate that the growth is not the same for the different studied parameters.

Fig. 10 shows the total entropy generation due to heat transfer (ST) in different power-law indexes, volume fractions, Rayleigh numbers and Darcy numbers. It is clear that the ST increases generally as the Rayleigh number and the volume fraction enhance in different power-law indexes and Darcy numbers. However, it demonstrates that the ST has different behavior in different Darcy numbers against various studied power-law indexes. At Da $= 0.001$, the ST enhances as the power-law index increases in various Rayleigh numbers. Moreover, it indicates that the effect of power-law index on the ST is more significant at Ra $= 10^5$ compared to 10^4. At Da $= 0.01$, the ST declines when the power-law index falls in various volume fractions at Ra $= 10^4$ and the drop is more sever from n $= 0.8$ and to 0.6. But, the ST augments as the power-law index decreases at Ra $= 10^5$. In addition, it shows that the effect of power-law index on the ST is more significant at Ra $= 10^4$ compared to 10^5. At Da $= 0.1$, the ST declines when the power-law index increases in various volume fractions and Rayleigh numbers and the drop is more considerable at Ra $= 10^5$.

6.3. Effects of power-law index, Darcy number, Rayleigh number and volume fraction on entropy generation due to fluid friction

Fig. 11 displays the local entropy generation due to fluid friction for pure fluid ($\varphi = 0$) and nanofluid ($\varphi = 0.04$) in different power-law indexes and Darcy numbers at Ra $= 10^5$ as maximum values of the local entropy generation is mentioned to provide a clear comparison between them. In mathematical view, it is clear from Eq. (30) that the increase in Darcy number enhances the entropy generation due to the fluid friction. Physically, as Darcy number increases, the hydraulic

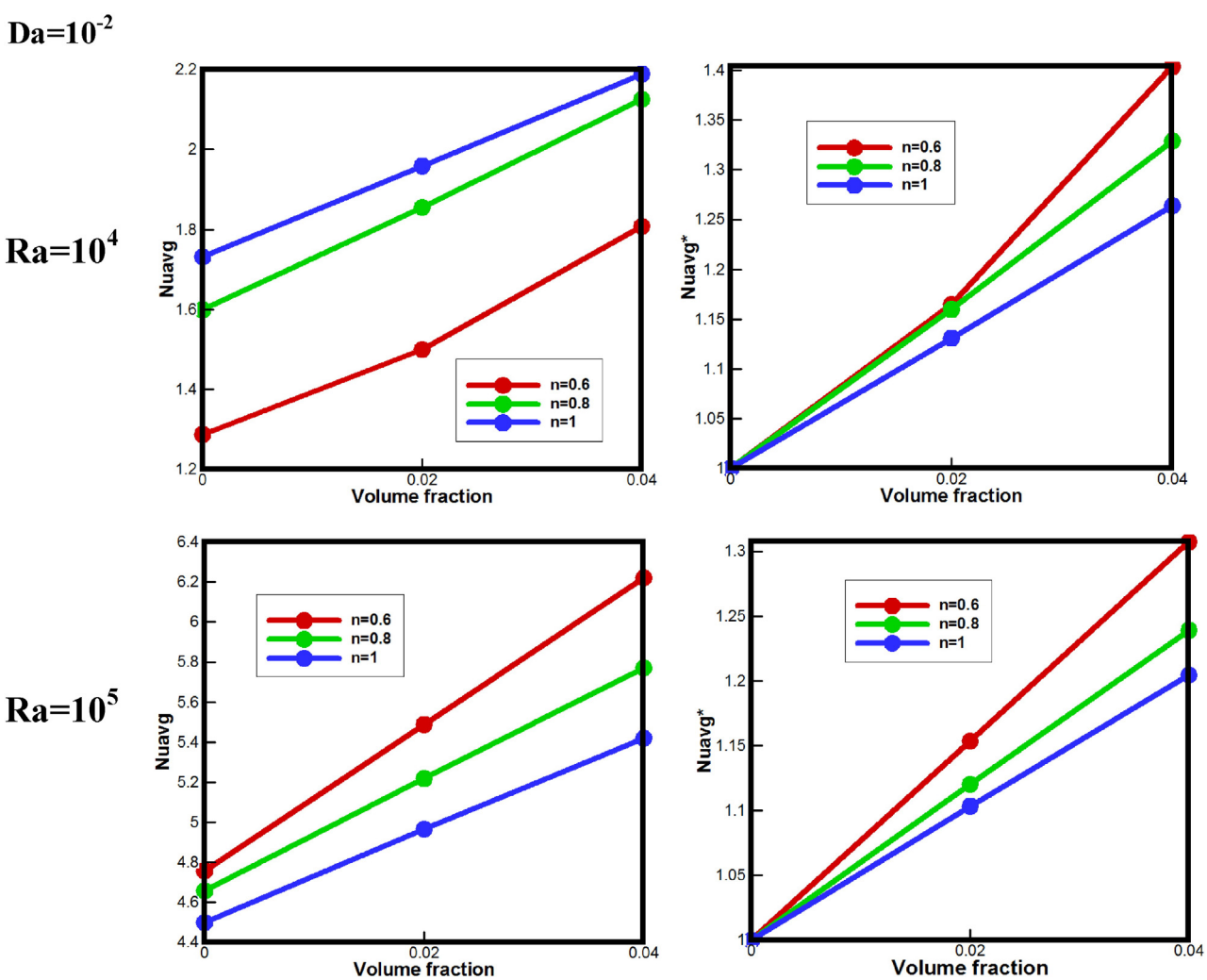

Fig. 8 (*continued*).

freepaper.me FREE paper

resistance of porous medium is reduced and the stronger fluid circulation is observed. Consequently, the irreversibility due to fluid friction is also found to increase. In addition, the distribution of the entropy shows that the entropy generation in the middle of the cavity becomes strong gradually with the enhancement of the Darcy number and the gradient of the entropy generation on the side wall augments hugely. The contours also show that distribution of the entropy is different compared to heat transfer generally where the considerable values of entropy could be observed on both horizontal walls in contrast with the heat transfer one. In fact, the presences of maximum values of horizontal velocity close to the horizontal walls causes the entropy to be observed in this section while the manner happens for sidewalls because of the maximum values of the vertical velocities near the sidewalls. It is obvious that the rise of power-law index not only alters the local entropy forms but also provokes the entropy amount to decrease noticeably. The comparison between fluid and nanofluid shows that the local entropy generation distribution in the cavity changes as the nanoparticles are added to the base fluid. In addition, the maximum values prove that the entropy due to fluid friction increases widely as a result of the added nanoparticles. At Da = 0.001, it is observable that the local entropy generation especially close to the left sidewall strengthens with the increase in the power-law index. For Da = 0.01, the augmentation of the power-law index provokes the entropy in different sections of the cavity to decrease and the drop is steady. On the other hand, the entropy generation due to fluid friction at Da = 0.1 plummets from n = 0.6 to 1 as the maximum entropy generation at n = 1 decreases by 46%.

Fig. 12 illustrates the total entropy generation due to fluid friction (SF), for pure fluid ($\varphi = 0$) and nanofluid ($\varphi = 0.04$) in different power-law indexes, volume fractions, Rayleigh numbers and Darcy numbers. It demonstrates that the SF enhances considerably as the Rayleigh number increases. In addition, the rise of the volume fraction augments the SF steadily in various power-law indexes and volume fractions. At Da = 0.001, the SF enhances as the power-law index increases in various Rayleigh numbers and volume fractions. Moreover, it indicates that the effect of power-law index on the SF is more significant at Ra = 10^4 compared to Ra = 10^5. At Da = 0.01, the SF declines when the power-law index falls in various volume fractions at Ra = 10^4; although, the drop is marginal from n = 1 to 0.8. But, the SF augments as the power-law index decreases at Ra = 10^5. In addition, it shows that the influence of power-law index on the SF is more noticeable at Ra = 10^4 compared with 10^5. At Da = 0.1, the SF declines when the power-law index increases in various volume fractions and Rayleigh numbers and the drop is more considerable at Ra = 10^5.

6.4. Effects of power-law index, Darcy number, Rayleigh number and volume fraction on the summation of entropy generations

Fig. 13 indicates the total local entropy generation due to fluid friction and heat transfer for pure fluid ($\varphi = 0$) and nanofluid ($\varphi = 0.04$) in different power-law indexes and Darcy numbers at Ra = 10^5 as maximum values of the local entropy generation are mentioned to provide a clear comparison between them. It is observed that the entropy

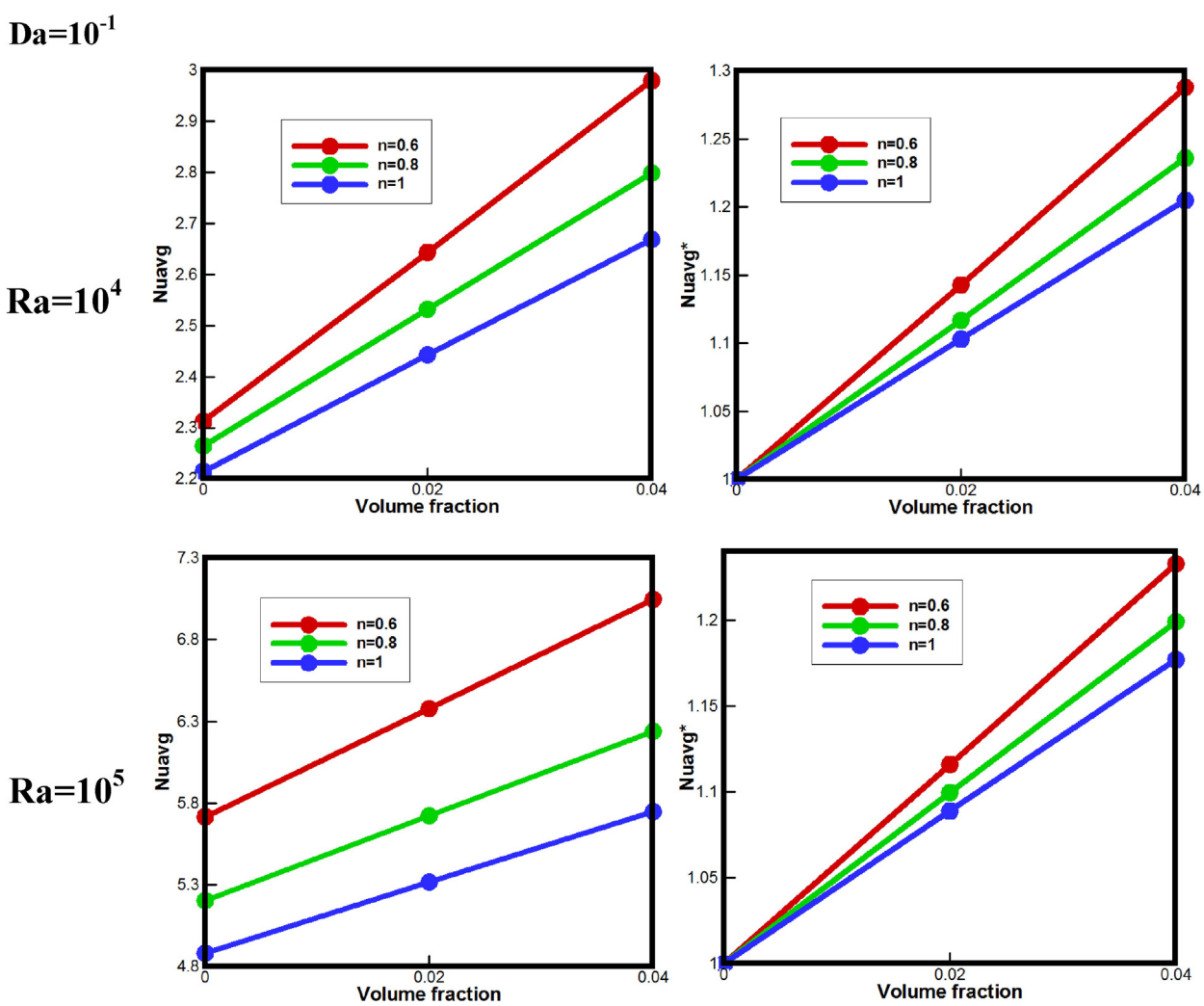

Fig. 8 (*continued*).

FREE paper freepaper.me دانلود کننده مقالات علمی

generation is strengthened by the increase in the Darcy number. In addition, the nanoparticle has a crucial role for enhancing the entropy generation in different power-law indexes and Darcy numbers. However, the effect of power-law index and the behavior of the total entropy generation are different in various Darcy numbers. At Da = 0.001, the trend of the total local entropy generation (S_S) is similar to the local entropy generation due to heat transfer (S_T) and it confirms that the S_T has a higher proportion in the S_S compared to S_F. Actually, it was predictable since the weakness of the fluid friction in low Darcy number (based on Eq. (30)) causes the S_T to be formed in the shape of S_s. In addition, it is

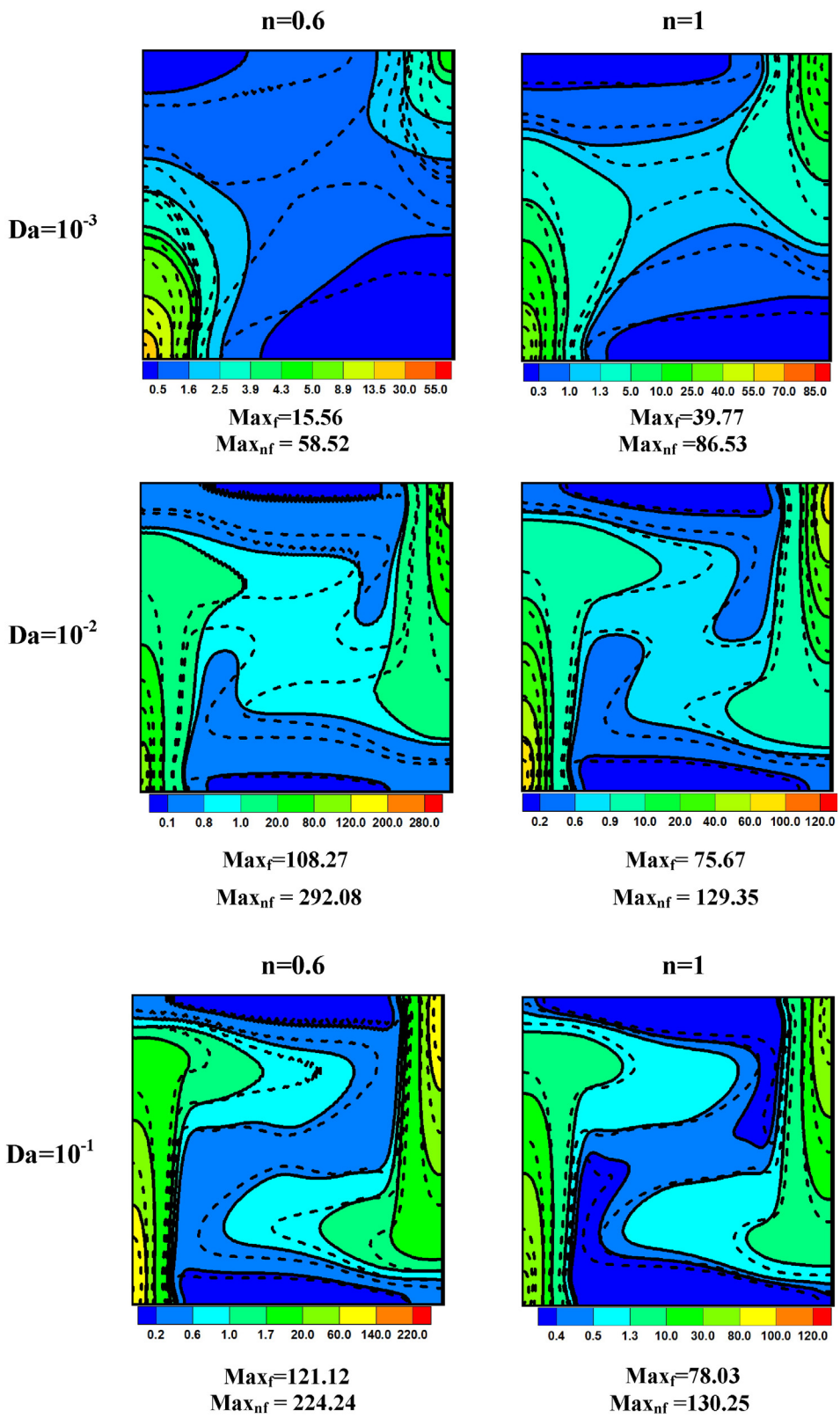

Fig. 9. Comparison of the local entropy generation due to heat transfer (S_T) between the base fluid (—) ($\varphi = 0$) and nanofluids (- - -) ($\varphi = 0.04$) for different Darcy numbers and power-law indexes at Ra = 10^5.

freepaper.me FREE paper

clear that the increase in the power-law index augments the irreversibilities considerably as it was found the enhancement of the power-law index rises the ST and SF separately. At Da = 0.01, the shape and distribution of the entropy generation are revolutionized where the high values of the irreversibility are generated close to the horizontal walls and demonstrate the influence of the fluid friction in the S_S. In fact, increase in the Darcy number provokes that role of the S_F to enhance in the S_S compared to Da = 0.001. In contrast with Da = 0.001, the enhancement of power-law index at Da = 0.01 has declined the total irreversibility and it is obvious in the displayed distribution and also the maximum values of the total entropy generation in the both pure fluid and the nanofluid. At Da = 0.1, the total entropy generation is completely similar to the S_F and the influence of the S_T on the S_S has been dropped considerably. Moreover, the rise of the power-law index has a diverse effect on the entropy generation as the S_S diminishes substantially with the increase of the power-law index from n = 0.6 to 1.

Fig. 14 exhibits the summation of the total entropy generation (SS) in various power-law indexes, volume fractions, Rayleigh numbers

freepaper.me FREE paper

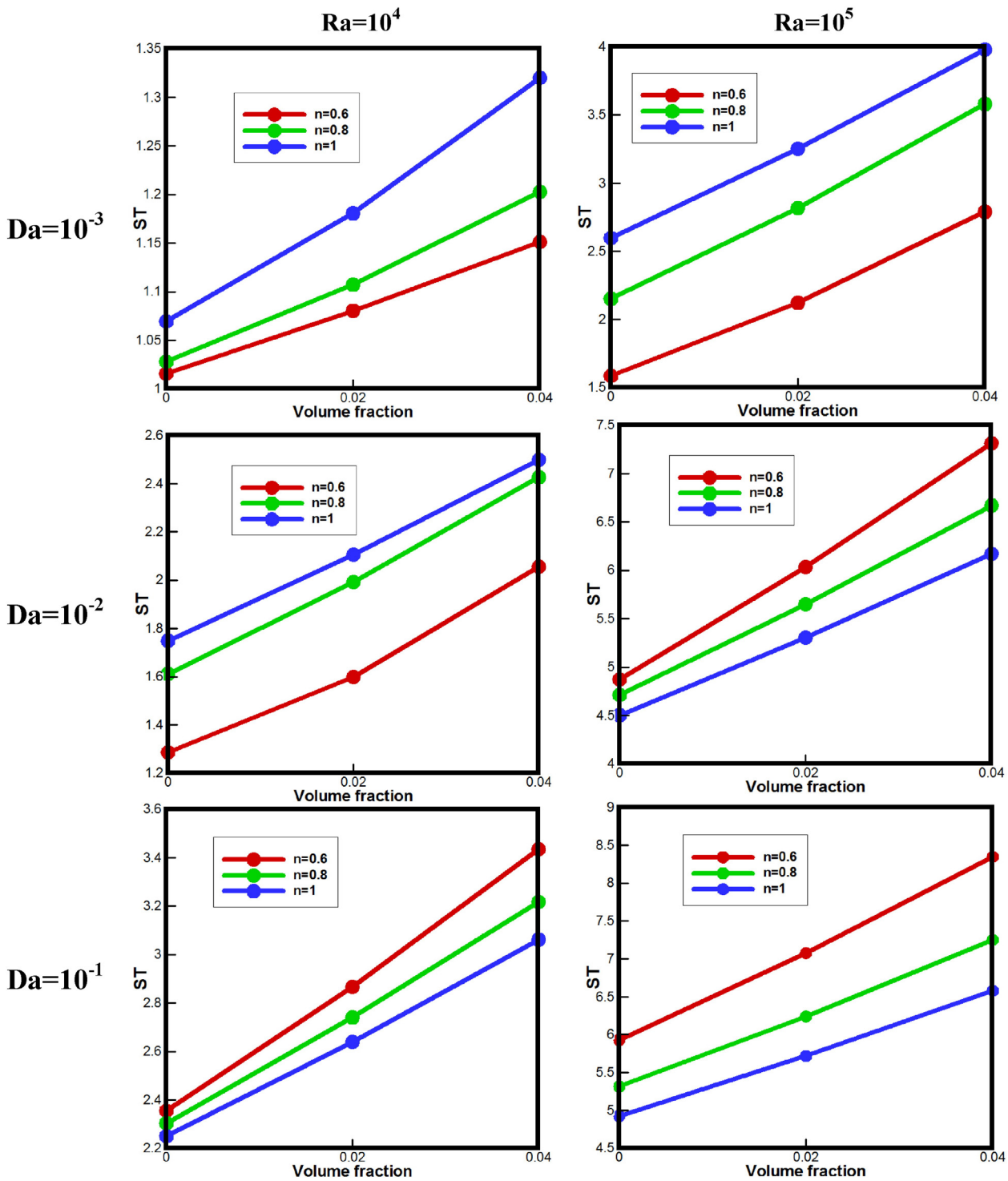

Fig. 10. Comparison between the total entropy generation due to heat transfer (ST) for various Rayleigh numbers, Darcy numbers, power-law indexes, and volume fractions.

and Darcy numbers. It shows the increase in the volume fraction enhances the SS gradually in different Rayleigh numbers, power-law indexes and Darcy numbers. In addition, the increase in Rayleigh number augments the SS for different Darcy numbers and power-law indexes. At Da = 0.001, the SS enhances as the power-law index increases in various Rayleigh numbers and volume fractions. Moreover,

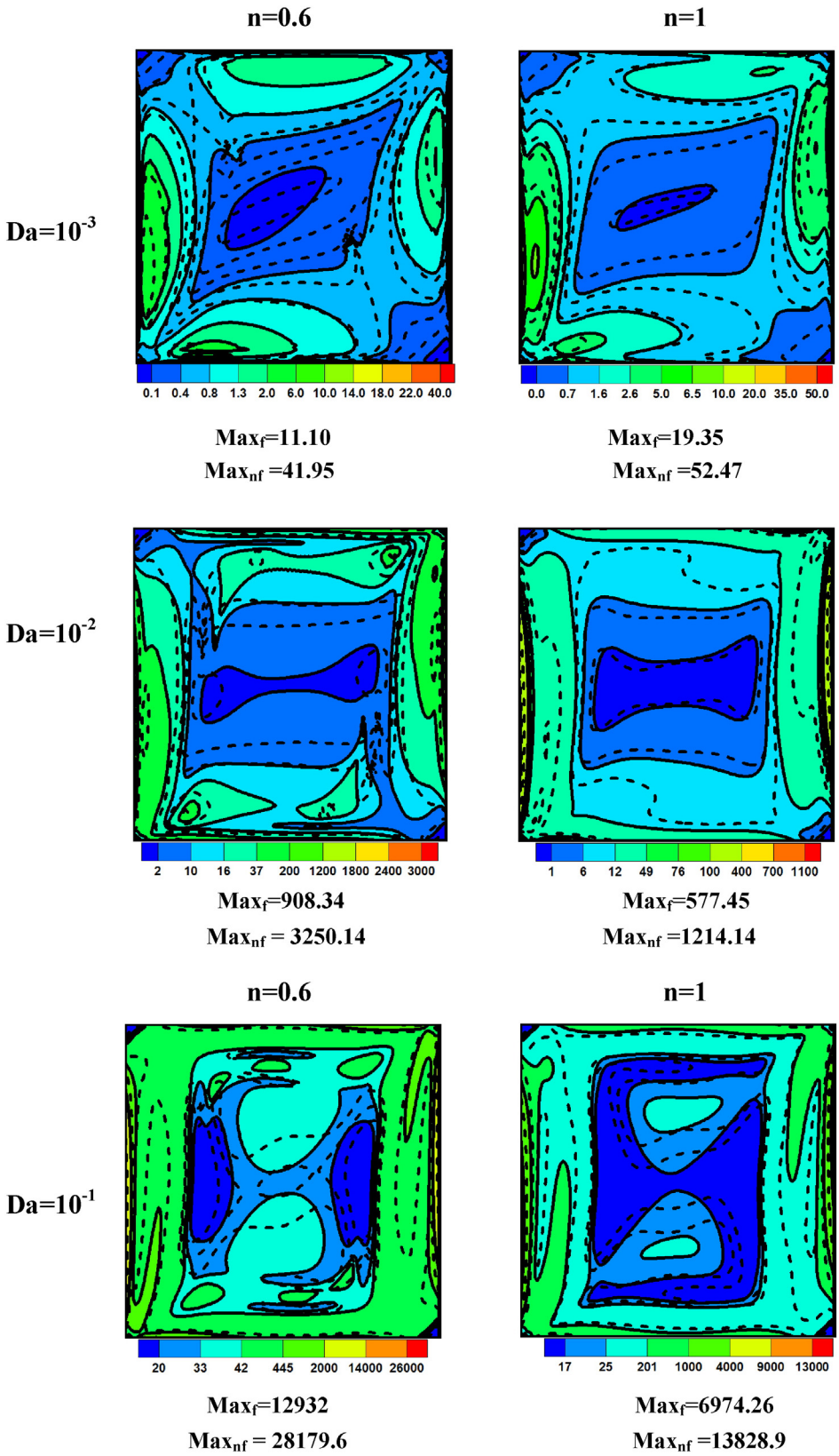

Fig. 11. Comparison of the local entropy generation due to fluid friction (S_F) between the base fluid (—) ($\varphi = 0$) and nanofluids (- - -) ($\varphi = 0.04$) for different Darcy numbers and power-law indexes at Ra = 10^5.

freepaper.me FREE paper

it indicates that the effect of power-law index on the SF is more significant from n = 0.8 to 1 at Ra = 10^4, but it occurs from n = 0.6 to 0.8 at Ra = 10^5. At Da = 0.01, the SS declines when the power-law index falls in various volume fractions at Ra = 10^4; although, the drop is marginal from n = 1 to 0.8. However, the SS augments as the power-law index decreases at Ra = 10^5. In addition, it shows that the effect of power-law index on the SS is more significant at Ra = 10^4 compared to 10^5. At Da = 0.1, the SS declines when the power-law index increases in various volume fractions and Rayleigh numbers and the drop is more considerable at Ra = 10^5.

6.5. Effects of power-law index, Darcy number, Rayleigh number and volume fraction on Bejan number

Fig. 15 shows local Bejan number for different power-law indexes, Darcy numbers, and volume fractions at Ra = 10^5. In fact, this figure reveals that the irreversibility because of heat transfer is dominant in which part of the cavity while the effects of the change into power-law index, Darcy number and volume fraction on the parameter have been illustrated. Generally, it indicates that the increase in the Darcy number causes the local Bejan number to weaken considerably in

FREE paper freepaper.me دانلود کننده مقالات علمی

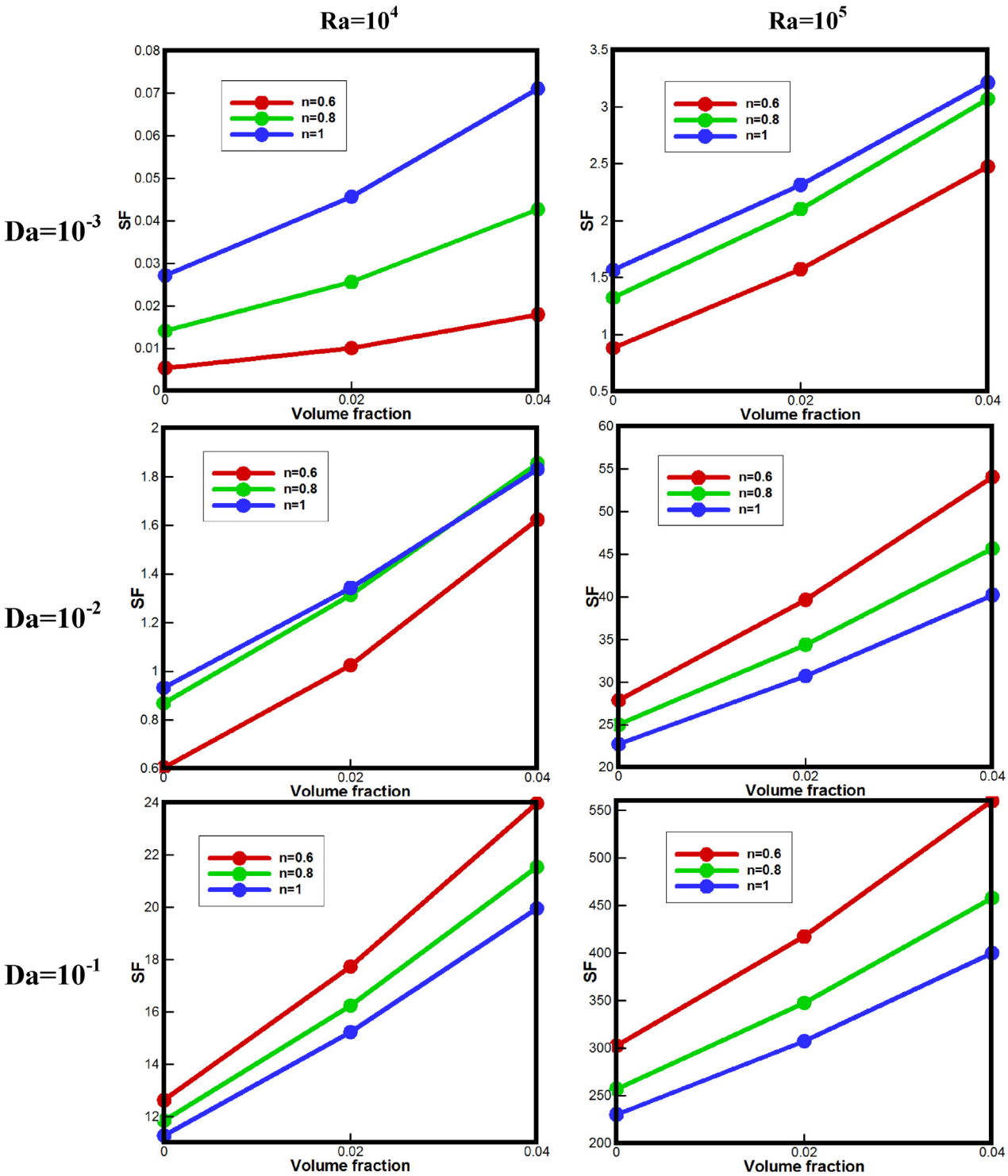

Fig. 12. Comparison of the total entropy generation due to fluid friction (SF) for various Rayleigh numbers, Darcy numbers, power-law indexes, and volume fractions.

different Rayleigh numbers and power-law indexes. In fact, the enhancement of the Darcy number augments the fluid friction and results in the drop of the effect of the entropy generation due to heat transfer. Hence, the Bejan number with consideration to Eq. (34) declines considerably as the Darcy number increase. Moreover, the enhancement of the volume fraction causes the local Bejan number to decrease and the maximum value section diminishes significantly in different power-law indexes and Darcy numbers. Nevertheless, the effect of power-law index on the local Bejan number is different in multifarious studied Darcy numbers. At Da = 0.001, the augmentation of the power-

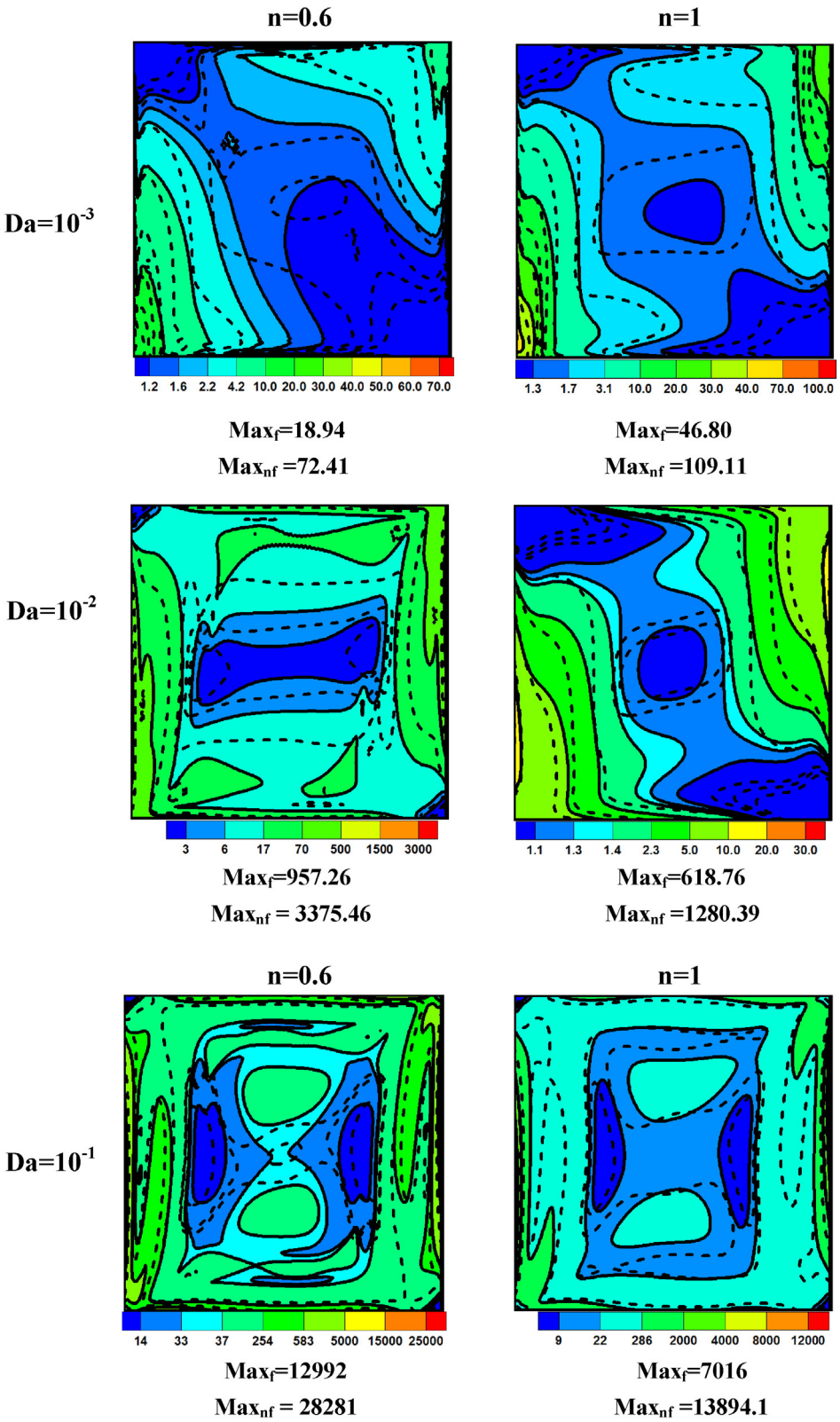

Fig. 13. Comparison of the total local entropy generation (S_S) between the base fluid (—) ($\varphi = 0$) and nanofluids (- - -) ($\varphi = 0.04$) for different Darcy numbers and power-law indexes at $Ra = 10^5$.

freepaper.me FREE paper

law index in this Darcy number has provoked the local Bejan number to weaken and interestingly, the drop is more noticeable in the pure fluid ($\varphi = 0$) where the maximum section in the middle of the cavity has been diminished considerably. At Da = 0.01 and 1, it is evident that the rise of the power-law index in the Darcy numbers have caused the local Bejan number to enhance.

Fig. 16 exhibits the average Bejan number in various power-law indexes, volume fractions, Rayleigh numbers and Darcy numbers. It illustrates that the average Bejan number decreases steadily as the volume fraction increases in various power-law indexes, Darcy numbers and Rayleigh numbers. In addition, the average Bejan number declines when the Darcy number augments in multifarious studied parameters. Moreover, the rise of the Rayleigh number causes the average Bejan number to decline considerably. However, the alteration of the power-law index has different effects on the average Bejan number in various Darcy and Rayleigh numbers. At Da = 0.001, the average Bejan number decreases with the enhancement of the power-law index for different Rayleigh numbers. However, the drop is minor from n = 0.8 to 1 at

FREE paper freepaper.me دانلود کننده مقالات علمی

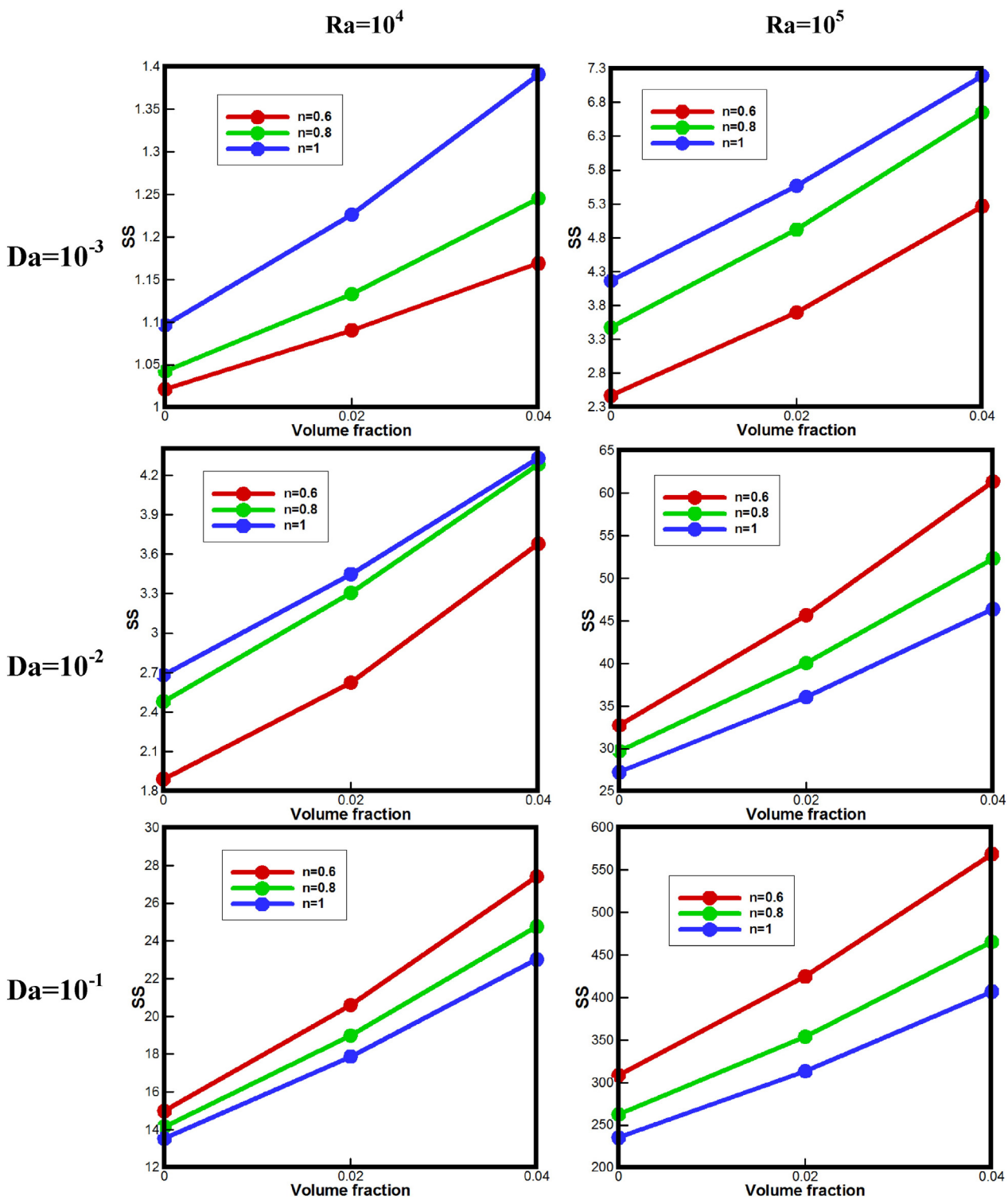

Fig. 14. Comparison of the summation of the total entropy generation (SS) for various Rayleigh numbers, Darcy numbers, power-law indexes, and volume fractions.

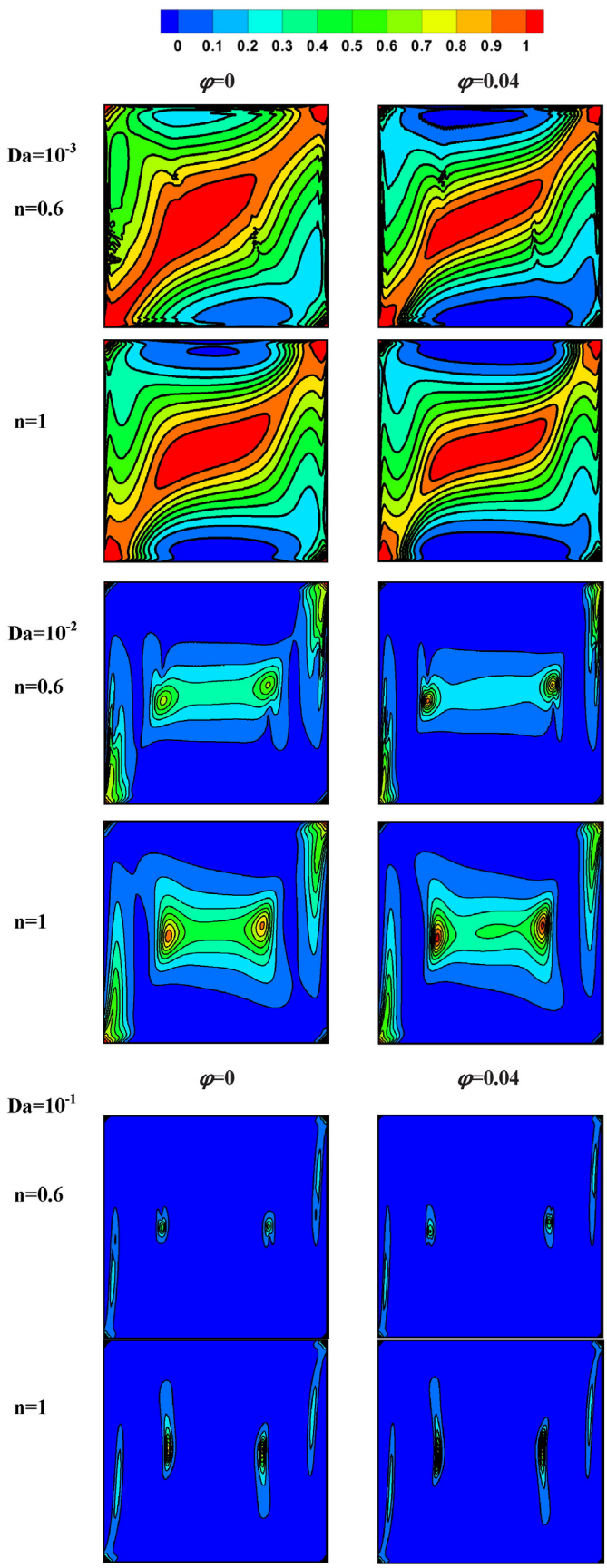

Fig. 15. Comparison of the local Bejan number (Be) between the base fluid and nanofluids for different Darcy numbers and power-law indexes at Ra = 10^5.

Ra = 10^5 and for nanofluids with the volume fraction of $\varphi = 0.04$, the values of n = 0.8 are more than n = 1. At Da = 0.01, the average Bejan number falls with the increase in the power-law index at Ra = 10^4; although, the amount of the average Bejan number is nearly the same for n = 0.8 and 1. In addition, the average Bejan number increases when the power-law index enhances at Ra = 10^5. At Da = 0.1, the augmentation of the power-law index augments the average Bejan number significantly in different Rayleigh numbers and volume fractions.

7. Conclusions

Heat transfer of natural convection in a porous cavity filled with non-Newtonian nanofluid has been studied and the entropy generations due to fluid friction and heat transfer are analyzed. Finite Difference Lattice Boltzmann Method (FDLBM) is utilized to simulate the problem. This study has been performed for the pertinent parameters in the following ranges: the Rayleigh number, Ra = 10^4 and 10^5, the power-law index, n = 0.6 to 1, Darcy number, Da = 10^{-3}–10^{-1} and the volume fractions, $\varphi = 0$ to 0.04. This investigation is analyzed for the various mentioned parameters and some conclusions are summarized as follows:

- The increase in Rayleigh number causes the average Nusselt number to enhance in various Darcy numbers, volume fractions and power-law indexes.
- The average Nusselt number increases when the Darcy number enhances for various power-law indexes, Rayleigh numbers, and volume fractions.
- The addition of the nanoparticle enhances the average Nusselt number. However, the effects of nanoparticles on the average Nusselt number are different in various Darcy numbers.
- At Da = 0.001, the average Nusselt number increases as the power-law index enhances in different Rayleigh numbers. In addition, the effects of nanoparticles enhance with the rise of the Rayleigh number for various power-law indexes in this Darcy number.
- At Da = 0.01, the average Nusselt number increases as the power-law index enhances at Ra = 10^4 while the average Nusselt number drops with the increase in the power-law index at Ra = 10^5. The enhancement of the power-law index declines the effects of nanoparticles.
- At Da = 0.1, the average Nusselt number augments when the power-law index decreases in different Rayleigh numbers. The enhancement of the power-law index declines the effects of nanoparticles.
- The enhancement of Rayleigh number augments different irreversibilities and causes the average Bejan number to drop considerably.
- The addition of nanoparticle enhances different entropy generations and declines the average Bejan number for different Rayleigh numbers, power-law indexes, and Darcy numbers.
- The increase in the Darcy number causes various entropy generations to rise for different power-law indexes and Rayleigh numbers. In addition, the enhancement of the Darcy number declines the average Bejan number
- At Da = 0.001, the increase in the power-law index enhances the entropy generations due to heat transfer and fluid friction in various Rayleigh numbers. Conversely, the average Bejan number drops with the enhancement of the power-law index.
- At Da = 0.1, the drop of the power-law index enhances the entropy generations due to heat transfer and fluid friction in different Rayleigh numbers. On the other hand, the average Bejan number augments as the power-law index increases.

Nomenclature

Be	Bejan number
c	Lattice speed
c_p	Specific heat at constant pressure
Da	Darcy number
F	External forces

freepaper.me FREE paper

f	Density distribution functions	n	Power-law index
f^{eq}	Equilibrium density distribution functions	N	The consistency coefficient
g	Internal energy distribution functions	Nu	Nusselt number
g^{eq}	Equilibrium internal energy distribution functions	P	Pressure
g_y	Gravity	Pr	Prandtl number
Gr	Grashof number	R	Gas constant
K	Permeability	Ra	Rayleigh number
L	The length of the cavity	T	Temperature

freepaper.me FREE paper

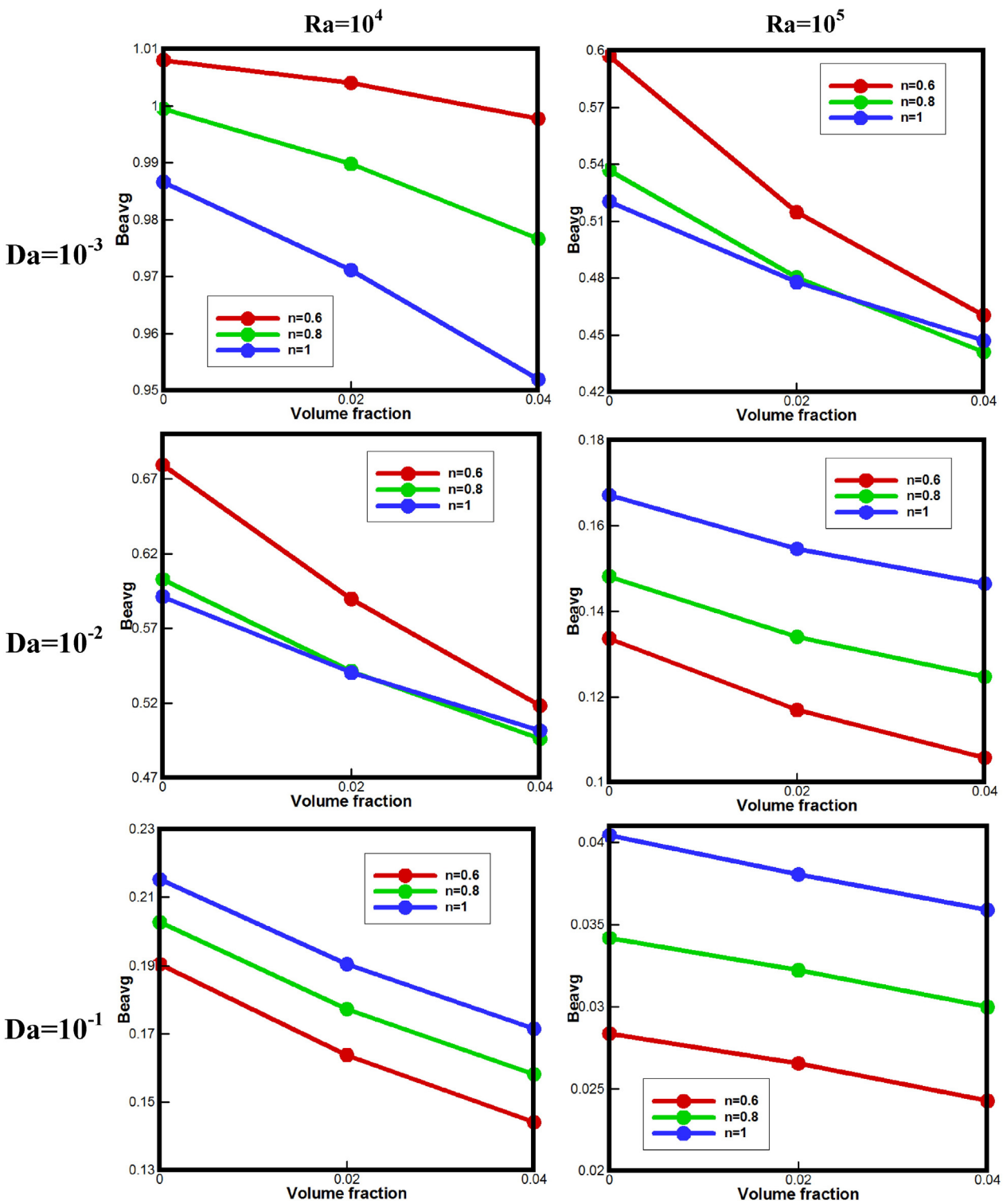

Fig. 16. Comparison of the average Bejan number (Be_{avg}) for different Rayleigh numbers, Darcy numbers, volume fractions and power-law indexes.

T_0	Bulk temperature ($T_0 = \frac{T_H+T_C}{2}$)
t	Time
x,y	Cartesian coordinates
u	Velocity in x direction
v	Velocity in y direction

Greek letters

φ	Solid volume fraction
β	Coefficient of volume expansion
ϕ	Relaxation time
τ	Shear stress
ζ	Discrete particle speeds
Δx	Lattice spacing
Δt	Time increment
α	Thermal diffusivity
ρ	Density
μ	Dynamic viscosity

Subscripts

avg	Average
C	Cold
H	Hot
x,y	Cartesian coordinates
α	The number of the node
T	Thermal
nf	Nanofluid
F, f	Fluid
s	Solid
S	Summation
tot	Total

References

[1] K. Khanafer, K. Vafai, M. Lightstone, Buoyancy-driven heat transfer enhancement in a two dimensional enclosure utilizing nanofluids, Int. J. Heat Mass Transf. 46 (2003) 3639–3653.

[2] H.F. Oztop, E. Abu-Nada, Numerical study of natural convection in partially heated rectangular enclosures filled with nanofluids, Int. J. Heat Fluid Flow 29 (2008) 1326–1336.

[3] G.H.R. Kefayati, S.F. Hosseinizadeh, M. Gorji, H. Sajjadi, Lattice Boltzmann simulation of natural convection in tall enclosures using water/SiO_2 nanofluid, Int. Commun. Heat Mass Transfer 38 (2011) 798–805.

[4] S.M. Aminossadati, B. Ghasemi, Natural convection of water–CuO nanofluid in a cavity with two pairs of heat source–sink, Int. Commun. Heat Mass Transfer 38 (2011) 672–678.

[5] M. Sheikholeslami, M. Gorji-Bandpy, S.M. Seyyedi, D.D. Ganji, H.B. Rokni, S. Soleimani, Application of LBM in simulation of natural convection in a nanofluid filled square cavity with curve boundaries, Powder Technol. 247 (2013) 87–94.

[6] A. Mahmoudi, I. Mejri, M.A. Abbassi, A. Omri, Lattice Boltzmann simulation of MHD natural convection in a nanofluid-filled cavity with linear temperature distribution, Powder Technol. 256 (2014) 257–271.

[7] M.S. Kandelousi, Effect of spatially variable magnetic field on ferrofluid flow and heat transfer considering constant heat flux boundary condition, Eur. Phys. J. Plus (2014) 129–248.

[8] M.S. Kandelousi, KKL correlation for simulation of nanofluid flow and heat transfer in a permeable channel, Phys. Lett. A 378 (45) (2014) 3331–3339.

[9] M. Sheikholeslami, Effect of uniform suction on nanofluid flow and heat transfer over a cylinder, J. Braz. Soc. Mech. Sci. Eng. 37 (2015) (1623-163).

[10] M. Sheikholeslami, T. Hayat, A. Alsaedi, MHD free convection of Al_2O_3–water nanofluid considering thermal radiation: a numerical study, Int. J. Heat Mass Transf. 96 (2016) 513–524.

[11] M. Sheikholeslami, K. Vajravelu, M.M. Rashidi, Forced convection heat transfer in a semi annulus under the influence of a variable magnetic field, Int. J. Heat Mass Transf. 92 (2016) 339–348.

[12] M. Sheikholeslami, R. Ellahi, Three dimensional mesoscopic simulation of magnetic field effect on natural convection of nanofluid, Int. J. Heat Mass Transf. 89 (2015) 799–808.

[13] M. Sheikholeslami, D.D. Ganji, Heat transfer of Cu–water nanofluid flow between parallel plates, Powder Technol. 235 (2013) 873–879.

[14] G. Domairry, M. Hatami, Squeezing Cu–water nanofluid flow analysis between parallel plates by DTM-Padé Method, J. Mol. Liq. 193 (2014) 37–44.

[15] A.R. Ahmadi, A. Zahmatkesh, M. Hatami, D.D. Ganji, A comprehensive analysis of the flow and heat transfer for a nanofluid over an unsteady stretching flat plate, Powder Technol. 258 (2014) 125–133.

[16] M. Hatami, D.D. Ganji, Natural convection of sodium alginate (SA) non-Newtonian nanofluid flow between two vertical flat plates by analytical and numerical methods, Case Stud. Therm. Eng. 2 (2014) 14–22.

[17] M. Hatami, M. Sheikholeslami, D.D. Ganji, Laminar flow and heat transfer of nanofluid between contracting and rotating disks by least square method, Powder Technol. 253 (2014) 769–779.

[18] M. Rahimi-Gorji, O. Pourmehran, M. Hatami, D.D. Ganji, Statistical optimization of microchannel heat sink (MCHS) geometry cooled by different nanofluids using RSM analysis, Eur. Phys. J. Plus 130 (2015) 1–12.

[19] M.A. Sheremet, I. Pop, Conjugate natural convection in a square porous cavity filled by a nanofluid using Buongiorno's mathematical model, Int. J. Heat Mass Transf. 79 (2014) 137–145.

[20] G.C. Bourantas, E.D. Skouras, V.C. Loukopoulos, V.N. Burganos, Heat transfer and natural convection of nanofluids in porous media, Eur. J. Mech. B. Fluids 43 (2014) 45–56.

[21] M.A. Sheremet, I. Pop, N. Bachok, Effect of thermal dispersion on transient natural convection in a wavy-walled porous cavity filled with a nanofluid: Tiwari and Das' nanofluid model, Int. J. Heat Mass Transf. 92 (2016) 1053–1060.

[22] U. Teipel, U. Förter-Barth, Rheology of nano-scale aluminum suspensions, Propellants Explos. Pyrotech. 26 (2001) 268–272.

[23] W.J. Tseng, C.H. Wu, Aggregation, rheology and electrophoretic packing structure of aqueous Al_2O_3 nanoparticle suspensions, Acta Mater. 50 (15) (2002) 3757–3766.

[24] M. Kole, T.K. Dey, Viscosity of alumina nanoparticles dispersed in car engine coolant, Exp. Thermal Fluid Sci. 34 (6) (2010) 677–683.

[25] H. Chen, Y. Ding, A. Lapkin, X. Fan, Rheological behaviour of ethylene glycol titanate nanotube nanofluids, J. Nanopart. Res. 11 (6) (2009) 1513–1520.

[26] P. Garg, J.L. Alvarado, C. Marsh, T.A. Carlson, D.A. Kessler, K. Annamalai, An experimental study on the effect of ultrasonication on viscosity and heat transfer performance of multi-wall carbon nanotube-based aqueous nanofluids, Int. J. Heat Mass Transf. 52 (21–22) (2009) 5090–5101.

[27] H. Chen, Y. Ding, A. Lapkin, Rheological behaviour of nanofluids containing tube/rod-like nanoparticles, Powder Technol. 194 (1–2) (2009) 132–141.

[28] T.X. Phuoc, M. Massoudi, Experimental observations of the effects of shear rates and particle concentration on the viscosity of Fe_2O_3-deionized water nanofluids, Int. J. Therm. Sci. 48 (7) (2009) 1294–1301.

[29] M. Hojjat, S.G. Etemad, R. Bagheri, J. Thibault, Rheological characteristics of non-Newtonian nanofluids: experimental investigation, Int. Commun. Heat Mass Transfer 38 (2011) 144–148.

[30] G.G. Ilis, M. Mobedi, B. Sunden, Effect of aspect ratio on entropy generation in a rectangular cavity with differentially heated vertical walls, Int. Commun. Heat Mass Transfer 35 (2008) 696–703.

[31] W.M. El-Maghlany, K.M. Saqr, M.A. Teamah, Numerical simulations of the effect of an isotropic heat field on the entropy generation due to natural convection in a square cavity, Energy Convers. Manag. 85 (2014) 333–342.

[32] M. Shahi, A.H. Mahmoudi, A.H. Raouf, Entropy generation due to natural convection cooling of a nanofluid, Int. Commun. Heat Mass Transfer 38 (2011) 972–983.

[33] M. Esmaeilpour, M. Abdollahzadeh, Free convection and entropy generation of nanofluid inside an enclosure with different patterns of vertical wavy walls, Int. J. Therm. Sci. 52 (2012) 127–136.

[34] C.C. Cho, C.L. Chen, C.K. Chen, Natural convection heat transfer and entropy generation in wavy-wall enclosure containing water-based nanofluid, Int. J. Heat Mass Transf. 61 (2012) 749–758.

[35] C.C. Cho, Heat transfer and entropy generation of natural convection in nanofluid-filled square cavity with partially-heated wavy surface, Int. J. Heat Mass Transf. 77 (2014) 818–827.

[36] M. Sheikholeslami, H.R. Ashorynejad, P. Rana, Lattice Boltzmann simulation of nanofluid heat transfer enhancement and entropy generation, J. Mol. Liq. 214 (2016) 86–95.

[37] G.H.R. Kefayati, FDLBM simulation of entropy generation due to natural convection in an enclosure filled with non-Newtonian nanofluid, Powder Technol. 273 (2015) 176–190.

[38] G.H.R. Kefayati, S.F. Hosseinizadeh, M. Gorji, H. Sajjadi, Lattice Boltzmann simulation of natural convection in an open enclosure subjugated to Water/copper nanofluid, Int. J. Therm. Sci. 52 (2012) 91–101.

[39] G.H.R. Kefayati, M. Gorji, D.D. Ganji, H. Sajjadi, Investigation of Prandtl number effect on natural convection MHD in an open cavity by Lattice Boltzmann Method, Eng. Comput. 30 (2013) 97–116.

[40] H. Sajjadi, M. Gorji, G.H.R. Kefayati, D.D. Ganji, Lattice Boltzmann simulation of turbulent natural convection in tall enclosures using Cu/Water nanofluid, Numer. Heat Transfer, Part A 62 (2012) 512–530.

[41] G.H.R. Kefayati, Effect of a magnetic source on natural convection in an open cavity subjugated to water/alumina nanofluid using Lattice Boltzmann Method, Int. Commun. Heat Mass Transfer 40 (2013) 67–77.

[42] G.H.R. Kefayati, Lattice Boltzmann simulation of MHD natural convection in a nanofluid-filled cavity with sinusoidal temperature distribution, Powder Technol. 243 (2013) 171–183.

[43] G.H.R. Kefayati, Lattice Boltzmann simulation of natural convection in nanofluid-filled 2D long enclosures at presence of magnetic source, Theor. Comput. Fluid Dyn. 27 (2013) 865–883.

[44] G.H.R. Kefayati, Lattice Boltzmann simulation of natural convection in partially heated cavities utilizing kerosene/cobalt ferrofluid, IJST, Trans. Mech. Eng. 37 (2013) 107–118.

[45] G.H.R. Kefayati, Simulation of ferrofluid heat dissipation effect on natural convection at an inclined cavity filled kerosene/cobalt utilizing Lattice Boltzmann Method, Numer. Heat Transfer, Part A 65 (2014) 509–530.

[46] G.H.R. Kefayati, Natural convection of ferrofluid in a linearly heated cavity utilizing LBM, J. Mol. Liq. 191 (2014) 1–9.

[47] H.R. Ashorynejad, A.A. Mohamad, M. Sheikholeslami, Magnetic field effects on natural convection flow of a nanofluid in a horizontal cylindrical annulus using Lattice Boltzmann method, Int. J. Therm. Sci. 64 (2013) 240–250.

دانلود کننده مقالات علمی freepaper.me FREE paper

[48] A. Abouei Mehrizi, M. Farhadi, S. Shayamehr, Natural convection flow of Cu–water nanofluid in horizontal cylindrical annuli with inner triangular cylinder using lattice Boltzmann method, Int. Commun. Heat Mass Transfer 44 (2013) 147–156.
[49] A. Abouei Mehrizi, M. Farhadi, K. Sedighi, M. Aghajani Delavar, Effect of fin position and porosity on heat transfer improvement in a plate porous media heat exchanger, J. Taiwan Inst. Chem. Eng. 44 (2013) 420–431.
[50] M. Jourabian, M. Farhadi, K. Sedighi, On the expedited melting of phase change material (PCM) through dispersion of nanoparticles in the thermal storage unit, Comput. Math. Appl. 67 (2014) 1358–1372.
[51] S.C. Fu, R.M.C. So, W.W.F. Leung, Linearized-Boltzmann-type-equation-based finite difference method for thermal incompressible flow, Comput. Fluids 69 (2012) 67–80.
[52] G.H.R. Kefayati, FDLBM simulation of magnetic field effect on non-Newtonian blood flow in a cavity driven by the motion of two facing lids, Powder Technol. 253 (2014) 325–337.
[53] G.H.R. Kefayati, Simulation of magnetic field effect on non-Newtonian blood flow between two-square concentric duct annuli using FDLBM, J. Taiwan Inst. Chem. Eng. 45 (2014) 1184–1196.
[54] G.H.R. Kefayati, Simulation of vertical and horizontal magnetic fields effects on non-Newtonian power-law fluids in an internal flow using FDLBM, Comput. Fluids 114 (2015) 12–25.
[55] G.H.R. Kefayati, Simulation of non-Newtonian molten polymer on natural convection in a sinusoidal heated cavity using FDLBM, J. Mol. Liq. 195 (2014) 165–174.
[56] G.H.R. Kefayati, FDLBM simulation of magnetic field effect on natural convection of non-Newtonian power-law fluids in a linearly heated cavity, Powder Technol. 256 (2014) 87–99.
[57] G.H.R. Kefayati, Simulation of magnetic field effect on natural convection of non-Newtonian power-law fluids in a sinusoidal heated cavity using FDLBM, Int. Commun. Heat Mass Transfer 53 (2014) 139–153.
[58] G.H.R. Kefayati, Mesoscopic simulation of magnetic field effect on natural convection of power-law fluids in a partially heated cavity, Chem. Eng. Res. Des. 94 (2015) 337–354.
[59] G.H.R. Kefayati, Mesoscopic simulation of double-diffusive mixed convection of pseudoplastic fluids in an enclosure with sinusoidal boundary conditions, Comput. Fluids 97 (2014) 94–109.
[60] G.H.R. Kefayati, Double-diffusive mixed convection of pseudoplastic fluids in a two sided lid-driven cavity using FDLBM, J. Taiwan Inst. Chem. Eng. 45 (2014) 2122–2139.
[61] G.H.R. Kefayati, et al., J. Mol. Liq. 198 (2014) 413–429.
[62] G.H.R. Kefayati, Mixed convection of non-Newtonian nanofluids flows in a lid-driven enclosure with sinusoidal temperature profile using FDLBM, Powder Technol. 266 (2014) 268–281.
[63] G.H.R. Kefayati, Simulation of heat transfer and entropy generation of MHD natural convection of non-Newtonian nanofluid in an enclosure, Int. J. Heat Mass Transf. 92 (2016) 1066–1089.
[64] G.H.R. Kefayati, Mesoscopic simulation of mixed convection on non-Newtonian nanofluids in a two sided lid-driven enclosure, Adv. Powder Technol. 26 (2015) 576–588.
[65] G.H.R. Kefayati, Magnetic field effect on heat and mass transfer of mixed convection of shear-thinning fluids in a lid-driven enclosure with non-uniform temperature boundary, J. Taiwan Inst. Chem. Eng. 51 (2015) 20–33.
[66] G.H.R. Kefayati, FDLBM simulation of magnetic field effect on mixed convection in a two sided lid-driven cavity filled with non-Newtonian nanofluid, Powder Technol. 280 (2015) 135–153.
[67] G.H.R. Kefayati, Mesoscopic simulation of magnetic field effect on Bingham fluid in an internal flow, J. Taiwan Inst. Chem. Eng. 54 (2015) 1–10.
[68] G.H.R. Kefayati, FDLBM simulation of mixed convection in a lid-driven cavity filled with non-Newtonian nanofluid in the presence of magnetic field, Int. J. Therm. Sci. 95 (2015) 29–46.
[69] G.H.R. Kefayati, "Simulation of double diffusive natural convection and entropy generation of power-law fluids in an inclined porous cavity with Soret and Dufour effects (Part I: study of fluid flow, heat and mass transfer), Int. J. Heat Mass Transf. 94 (2016) 539–581.
[70] G.H.R. Kefayati, "Simulation of double diffusive natural convection and entropy generation of power-law fluids in an inclined porous cavity with Soret and Dufour effects (Part II: entropy generation), Int. J. Heat Mass Transf. 94 (2016) 582–624.
[71] B. Goyeau, J.P. Songbe, D. Gobin, Numerical study of double-diffusive natural convection in a porous cavity using the Darcy–Brinkman formulation, Int. J. Heat Mass Transf. 39 (1996) 1363–1378.
[72] B. Tanmay, S. Roy, T. Paul, I. Pop, Natural convection in a square cavity filled with a porous medium: effects of various thermal boundary conditions, Int. J. Heat Mass Transf. 49 (2006) 1430–1441.
[73] S.K. Pandit, A. Chattopadhyay, Higher order compact computations of transient natural convection in a deep cavity with porous medium, Int. J. Heat Mass Transf. 75 (2014) 624–636.
[74] P.D. Lax, B. Wendroff, Systems of conservation laws, Commun. Pure Appl. Math. 13 (1960) 217–237.

دانلود کننده مقالات علمی freepaper.me FREE paper